Contribution of Western Arabian Sea Tropical cyclones to rainfall in the Horn of Africa.

P. Camberlin [1], O. Assowe [2], B. Pohl [1], M. Mohamed Waberi [1, 2], K. Hoarau [3], O. Planchon [1]

[1] Centre de Recherches de Climatologie, UMR 6282 Biogéosciences, CNRS/Université de Bourgogne, Dijon, France.

[2] Observatoire Régional de Recherche sur l'Environnement et le Climat (ORREC), Centre d'Etudes et de Recherche de Djibouti (CERD), Djibouti-ville, République de Djibouti.

[3] PLACES, CY Cergy Paris Université, France

Submitted to Journal of Geophysical Research : Atmospheres

28 February 2024

Abstract

The occurrence of tropical cyclones (TC) in the Horn of Africa and nearby areas is for the first time examined to document their contribution to local rainfall and their trends over the period 1990-2020. An average 1.5 TC (of any intensity) per year was observed over the Western Arabian Sea, with two asymmetrical seasons, namely May-June (30% of cyclonic days) and September-December (70%). Case studies reveal that in many instances, TC-related rainfall extends beyond 500 km from the TC center, and that substantial rains occur one to two days after the lifecycle of the TC. Despite their rarity, in the otherwise arid to semi-arid context characteristic of the region, TCs contribute in both seasons to a very high percentage of total rainfall (up to 30 to 60%) over the northwestern Arabian Sea, the Gulf of Aden and their coastlines. Over inland northern Somalia, contributions are much lower. TCs disproportionately contribute to some of the most intense daily falls, which are often higher than the mean annual rainfall. A strong increase in the number of TCs is found from 1990 to 2020, hence their enhanced contribution to local rainfall. This increase is associated with a warmer eastern / southern Arabian Sea, a decrease in vertical wind shear, and a strong increase in tropospheric moisture content.

1. Introduction

Tropical cyclones (TCs) develop over sufficiently warm off-equatorial oceanic regions, which are generally wet areas receiving well over 1000 mm of precipitation per year. Although the Arabian Sea is not among the most active cyclonic basins, accounting, together with the Bay of Bengal, for only 4-6% of the world's TCs (Ramsay, 2017; Neumann, 2017 ; Singh and Roxy, 2022), it stands out by its low mean annual rainfall, which does not exceed 500 mm in its northwestern half. Very few other arid regions, like northwestern Mexico (Fors, 1977; Breña-Naranjo et al., 2015) and Western Australia (Ng et al., 2014), similarly experience TCs. Although considered a very rare occurrence along the coasts of northern Somalia, Yemen, and to some extent Oman (Pedgley, 1969; Al-Manji, 2021), the recent past provided evidence of several high intensity systems, e.g. the "very severe cyclonic storms" Gonu in 2007, Chapala and Megh in 2015, Mekunu and Luban in 2018. Their landfall in arid environments provides unusually high rainfall amounts in a short period of time, which have major short-term consequences (e.g., flash floods destroying infrastructure, settlements, claiming lives and killing livestock) as well as longer-term impacts, for instance on groundwater recharge (Abdalla and Al-Abri, 2011) and the dynamics of endangered tree species (Lvoncik et al., 2020). In the late 2010s, the succession of several unusually wet seasons, in which TCs played a dominant role, induced the worst locust outbreak of the last decades in Southern Arabia and the Horn of Africa (Salih et al., 2020 ; Owuor and David-McRae, 2022). In the Republic of Djibouti alone, the desert locust infestation in 2019-2020 caused a loss of 5 million USD over crops and pastures. Even moderately strong tropical systems have large impacts because of the associated heavy rains. For instance, cyclonic storm Sagar brought 181 mm of rainfall in Djibouti-city on two days in May 2018, extensively flooding huge urban neighbourhoods and schools, and destroying transportation and sanitation infrastructures (Cherel et al., 2020). The low income populations of the Horn of Africa, usually confronted to harsh climatic conditions related to recurrent droughts, are particularly vulnerable to such high intensity rainfall events, yet to the best of our knowledge there has never been any systematic study of how frequently TCs affect this part of the continent.

Over the Western Arabian Sea (WAS hereafter) and neighbouring coastal areas (Yemen, Somalia, Djibouti), more generally, the average contribution of TCs to local rainfall is little known. Pedgley (1969) found that at Salalah (southern Oman), a quarter of the total rainfall from 1943 to 1967 was associated with cyclones. Jiang and Zipser (2010) and Prat and Nelson (2013) quantified the contribution of tropical storms to global precipitation from TRMM data. Over the period 1998-2006, it varied from 3 to 11% depending on the basins (Jiang and Zipser, 2010), and 5% for the North Indian Ocean basin which includes both the Bay of Bengal and the Arabian Sea. Comparable values were obtained by Prat and Nelson (2013) using 12 years of data from 1998 to 2009. Much higher contributions were found over localised areas such as the coasts of Baja California in Mexico (Breña-Naranjo et al., 2015) and

northwest Australia (Ng et al., 2014), but they decrease significantly within the first 150 km from the coast (Prat and Nelson, 2013). Khouakhi et al. (2017) examined the contribution of TCs to rain-gauge precipitation amounts and found that they account for a large portion (35-50%) of mean annual rainfall in a few regions including northwestern Australia, southeastern China, the northern Philippines, and northwestern Mexico. However, their study did not document the Arabian Sea area. Prat and Nelson (2013) published a map covering the North Indian Ocean basin, but due to the small number of years, the TC-related rainfall contribution is relatively noisy over the WAS. Kabir et al. (2022) studied TC exposure in the North Indian Ocean. TC-associated rainfall is much higher around the Bay of Bengal sub-basin than over the Arabian Sea, partly due to the larger number of TCs making landfall around the Bay of Bengal (155 between 1989 and 2018, as compared to 30 around the Arabian Sea). Nevertheless, the latter have a high contribution to TRMM total rainfall along the southeastern coasts of Arabia, reaching 50% in parts of Oman (Kabir et al. 2022).

The objectives of the present study are to quantify the mean rainfall amount resulting from TCs in the WAS, Gulf of Aden and riverine countries (Somalia, Djibouti, Yemen), and their contribution to the total rainfall amounts, which have never been comprehensively analysed before, since all previous studies on TC-induced precipitation were actually carried out at a much broader scale. Daily rainfall extremes associated with TCs will also be examined and compared to local absolute 24-hr maxima. Some case studies of TCs making landfall over the coasts of Somalia and Djibouti will also be presented in order to better apprehend the spatial distribution of rainfall during such events and its relationship to the storms size and track. A better knowledge of TCs in the region and their contribution to the local climatology is an important issue, because several studies point to a recent (Wang et al. 2012 ; Murakami et al. 2017 ; Baburaj et al. 2020 ; Deshpande et al. 2021 ; Priya et al., 2022 ; Tiwari et al. 2022) and forthcoming increase (Murakami et al. 2013 ; Knutson et al. 2015 ; Bell et al. 2020) in the frequency of Arabian Sea TCs. While Murakami et al. (2013) attributed the recent increase to anthropogenic climate change, more ambiguous results were obtained by Wang et al. (2023). Evan et al. (2011) found that a recent increase in storm intensity could have been driven by enhanced anthropogenic black carbon and sulphate emissions, resulting in a reduction of vertical wind shear, but this was challenged by Wang et al. (2012).

Besides documenting the patterns of TC-related rainfall over the north-eastern tip of Africa and adjacent regions, the present study analyses trends of TC-related and total rainfall over the last 20-30 years. Given the major changes found in TC occurrence in the last decades, a comparison is also made of the regional oceanic and atmospheric conditions which may have triggered these changes. Section 2 presents the cyclone and precipitation data used in the study. The TC and precipitation climatologies are depicted in section 3.1, followed by the selected TC case studies (3.2). The statistical analysis of

mean rainfall amounts associated with TCs is then presented (3.3), before an appraisal of TC-related rainfall trends since 1990 (3.4) and the associated oceanic and atmospheric conditions (3.5).

2. Data and methods

2.1 Cyclone tracks

Data on 3-hourly North Indian Ocean TC locations were extracted from the IBTrACS (International Best Track Archive for Climate Stewardship, Knapp et al., 2010 & 2018) dataset. All observations west of 75°E were retained. This is slightly further east than the WAS target area (33-65°, 0-22°N) because it is necessary to extract TC-related rainfall over a wide radius from the TC center. Given that some of the rainfall data are at daily timescale, the successive locations of each cyclone are averaged over each 24-hr period. As discussed below, the wide radius which will be retained around the TC center accommodates the TC propagation within each day.

All TC categories were retained in the study, i.e. including weak systems like tropical depressions (wind speeds between 17 and 34 knots). Substantial rains are sometimes associated with tropical depressions, which justifies the inclusion of these weaker systems. For instance, Arabian Sea tropical depression 02A, with weak maximum sustained winds (25 knots), which in 2008 made landfall in Yemen, caused widespread flooding, 180 deaths and 22 000 displaced people (Evan and Camargo, 2011). Some analyses will be separately carried out on the Very Severe Cyclonic Storms (VSCS hereafter), the third highest category used by the India Meteorological Department to classify North Indian Ocean tropical cyclones, and which is equivalent to the Hurricane category (winds of at least 64 knots). Hereafter, TC refers to all categories of disturbances, not just VSCS.

The study is restricted to the period from 1990 (2000 for some analyses) to 2020. Data for the pre-satellite era over the North Indian Ocean are not fully reliable due to a possible undercount of TCs (Evan and Camargo, 2011 ; Singh et al. 2020 ; Deshpande et al. 2021 ; Wahiduzzaman et al. 2022). Additionally, Kabir et al. (2022) and Tiwari et al. (2022) warned that TC records over the North Indian Ocean may not be fully complete prior to 1990 due to missing intensity records. Hoarau et al. (2012) re-analysed TC data over the Northern Indian Ocean using the Dvorak (1984) method. They warned of a probable undercount of intense TCs during 1980-1989. From 1990 onwards, the agreement between North Indian Ocean TC track-data from the Indian Meteorological Department (IMD) and the Joint Typhoon Warning Center (JTWC) greatly improved (Evan and Camargo, 2011 ; Schreck et al. 2014), suggesting that working on this period is less uncertain.

2.2 Precipitation data

Two daily gridded precipitation datasets based on satellite information calibrated with some ground data were used and complemented by rain-gauge data for northern Somalia and Djibouti. The gridded datasets were selected to document both land and oceanic areas, at a relatively high spatial resolution.

PERSIANN-CDR (Precipitation Estimation from Remotely Sensed Information using Artificial Neural Networks–Climate Data Record – Ashouri et al., 2015) uses infrared satellite data as the main input, from which a neural network model is developed whose parameters are based on radar data. The resulting rainfall estimates are next calibrated using the monthly Global Precipitation Climatology Project (GPCP) data. The product is available from 1 January 1983 to the present, at 0.25° spatial resolution.

IMERG (Integrated Multi-satellitE Retrievals for the Global Precipitation Measurement, Huffman et al. 2015) is a gridded rainfall product with global coverage, based on NASA's precipitation algorithm, applied to data from the TRMM (Tropical Rainfall Measurement Mission) and the GPM (Global Precipitation Measurement) satellite missions. It covers the period from 2000 to the present day, at a high spatial (0.1 degree) and temporal (30 minute) resolution. The input data include passive microwave (PMW) precipitation estimates, considered as more direct retrievals, calibrated to the combined radar-radiometer product from TRMM and GPM. An interpolation of the PMW estimates is performed by propagating them forward and backward in time using motion vectors. The resulting estimates are further combined to infrared (IR) precipitation estimates, and a final bias adjustment to rain-gauge observations is made over land areas.

For both data sets, the region 3°S-22°N, 35-65°E, i.e. the Greater Horn of Africa (GHA) and nearby regions, was extracted. The period retained is 1990-2020 (2000-2020 for IMERG) to take into account TC data reliability as exposed above. Note that, unless otherwise stated, the results obtained for PERSIANN and IMERG are qualitatively similar, hence will not be systematically duplicated. Below, IMERG is generally preferred to PERSIANN, because it slightly better agrees with rain-gauge data.

Daily rain-gauge data for 25 stations in Northern Somalia (mainly Somaliland and Puntland areas) were obtained from SWALIM (Somalia Water and Land Information Management), a project managed by FAO. The period covered is 2005-2020, with data availability varying from 10 to 16 years. For the Republic of Djibouti, data from Djibouti-Airport station, with complete daily rainfall records between 2000 and 2020, were obtained from the National Meteorological Agency of Djibouti.

2.3 Methods for quantifying TC-associated precipitation

Quantifying the contribution of TCs to rainfall requires defining to what distance of the TC center rainfall is considered as being related to the TC. Most studies consider a 500 km radius (e.g., Jiang and

Zipster, 2010 ; Prat and Nelson, 2013; Lavender and McBride, 2021). This threshold is meant to be within the range of the outer edge of the TC cloud shield (550–600 km) (Englehart et al. 2001, Kabir et al. 2022). Rather than blindly adopting the same threshold, mean daily rainfall was plotted as a function of distance to the TC center, for all TCs reported in the period 2000-2020 in the WAS area. Boxplots were constructed to derive the median rainfall and its variability for 40 km bins (section 3.3). From these plots an adapted threshold was defined, and all rainfall which fell within this distance from the TC center was considered as TC-related. Rainfall in the days immediately following the demise of each TC was also examined in order to find out whether part of it can be ascribed to remnants of the disturbance. This procedure was used to quantify TC-related rainfall for each disturbance, and to compute statistics for the period 2000-2020 based on the gridded PERSIANN and IMERG rainfall estimates, and the stations available in the years 2005-2020 in Northern Somalia and Djibouti.

The contribution of TC-related rainfall to total rainfall was computed. To document the part played by TCs on intense rainfall, days recording above 30 mm were extracted and the proportion which are TC-induced was computed. Maximum 24-hr rainfall at available rain-gauges was also examined to assess to which extent it relates to TC occurrence. These analyses were carried out separately on the two cyclonic seasons, i.e. the pre-monsoon (May-June) and the post-monsoon (September-December).

Rainfall trends over the period 2000-2020 (extended to 1990-2020 for PERSIANN) were mapped for total rainfall, TC-related rainfall, non-TC related rainfall and the contribution of TC-related rainfall to total rainfall amounts. Mann-Kendall Tau statistics were computed to assess the statistical significance of the trends.

3. Results

3.1 Rainfall and TC climatologies

The region around the northeastern tip of Africa is mostly an arid to semi-arid area, with less than 500 mm/yr (fig.1). Mean annual rainfall (MAR) increases to the southeast, in the Central Indian Ocean, in the west over highland areas (Ethiopia, Kenya, Yemen), and along a narrow subcostal belt stretching northward from Southern Kenya. The region covering most of South Arabia, the Gulf of Aden and neighbouring areas is particularly arid (less than 200 mm/yr), with no well-defined rainy season. Much of Somalia and its surroundings have two brief rainy seasons, in March-May and October-November. Due to the divergence of large-scale air flows, most of the region experiences dry boreal winters (December-February) and summers (June-September), the main exception being the Ethiopian highlands.

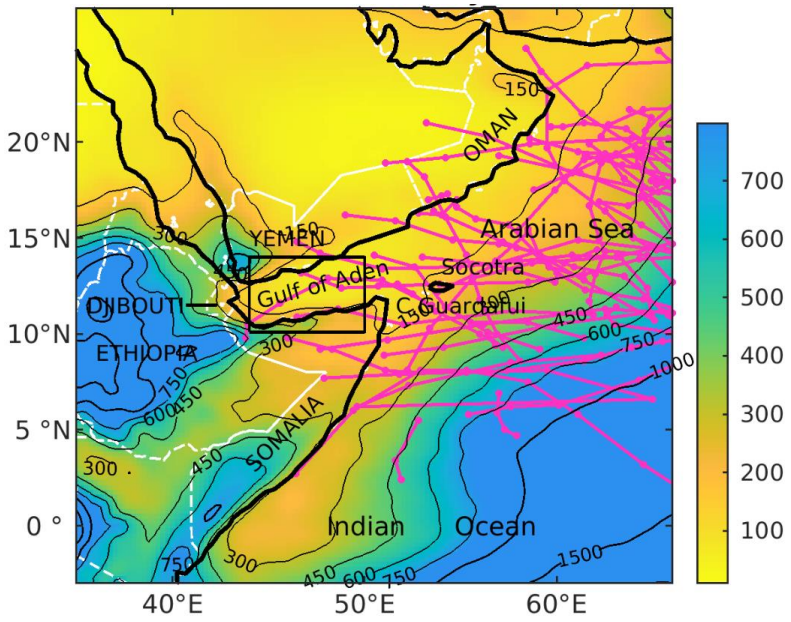

Figure 1 : Location map, with shadings representing mean annual rainfall (PERSIANN data, 1990-2020, in mm) and pink lines TC tracks (same period). The box shows the area over which the Gulf of Aden rainfall index is computed (section 3.4).

From 1990 to 2020, a total of 47 TCs crossed the WAS, with a mean life-time (within the region) of 4.6 days. The number of TCs gradually decreases from east to west (fig.2), with tracks generally showing E-W or SE-NW directions. A minority of the TCs display more meridional tracks, with southerly propagations on rare occasions (e.g. TC Kyarr in 2019). Only about a third of these TCs made landfall over the continent, either on the coasts of Southern Arabia or on those of Somalia, with a few additional TCs which approached close to the coasts or crossed Socotra island. A small proportion of these disturbances belong to the VSCS category. On average, only 1.1 days.year^{-1} record a VSCS, as compared to 7.1 days.year^{-1} for all TC categories.

TCs reaching or developing over the WAS are found in two distinct seasons (fig.2), which correspond to the pre-monsoon season (May-June) and post-monsoon season (September-December, clearly peaking in October-November). During the monsoon season (boreal summer), the strong wind shear between the low-level westerlies and the upper-tropospheric Tropical Easterly Jet, as well as lower SST over parts of the WAS, disable the development of TCs (Gray, 1968 ; Evan and Camargo, 2011 ; Baburaj et al. 2020). TCs are much less frequent in May-June (MJ) than in September-December (SOND). The latter season makes up about two thirds of the number of TCs, and 70% of the cyclonic days. This is specific to the WAS: for the Arabian Sea as a whole the number of TCs is approximately the same in the two seasons (Evan and Camargo, 2011), with some decadal variations (Al-Manji et al. 2021). The smaller number of pre-monsoon TCs in the western part of the Arabian Sea compared to post-monsoon has rarely been highlighted (Ray-Choudhuri et al. 1959), though it is obvious in Singh and

Roxy (2022, their figure 3). There is no current explanation for this difference, but it is not related to SST, which are higher in the pre- than in the post-monsoon seasons. Dynamical conditions could be more conducive to a westward motion of the TCs initiated over the eastern Arabian Sea. The predominantly east-west tracks of many of the post-monsoon TCs is shown on figure 2a. May-June tracks are slightly more uneven, and few of them make landfall over northeastern Africa or southern Arabia.

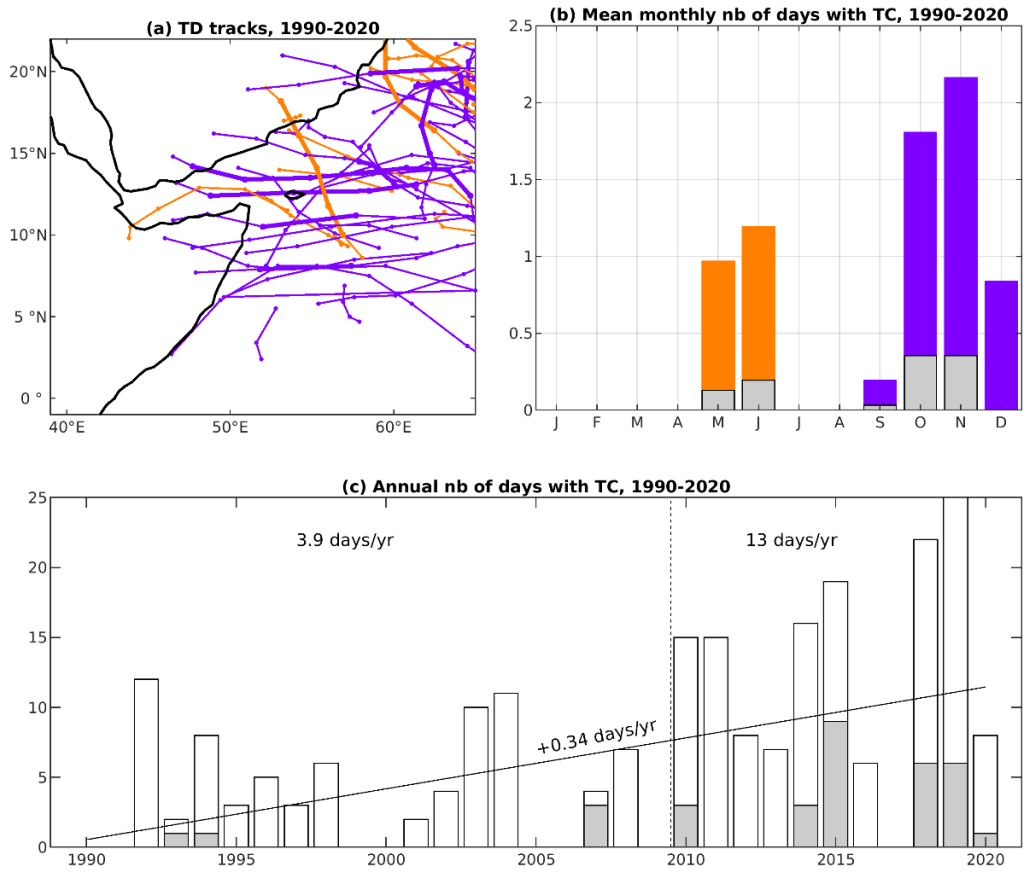

Figure 2 : TC tracks and TC statistics for the Western Arabian Sea, 1990-2020. Orange colours refer to the May-June season, purple colours to the September-December season. Grey bars in panels (b) and (c) stand for VSCS, which are identified by bold lines in panel (a). In panel (c), white bars show the yearly total of TC days (TC center located west of 65°E), with the linear trend computed as Sen's slope. The vertical dashed line is the breaking point according to Pettitt's test ($p<0.01$), with the mean number of TC days for the two sub-periods in the top part of the panel.

Large interannual variations are found in the number of TC days (fig. 2c). In some years, no TCs are recorded in the WAS. There has been a clear and strong positive trend in the number of TC days in the period 1990-2020 (+0.34 per year, significant at $p<0.01$), corroborating Deshpande et al. (2021). Pettitt's test for change-point detection indicate a significant upward increase ($p<0.01$) after 2009. In the first sub-period (1990-2009), there was an average of 3.9 TC days/year in the WAS, rising to 13

days/year between 2010 and 2020. Statistics for WSCS are less robust, given the rare occurrence of disturbances in this category. While these storms were exceptional between 1990-2009, they became much more common from 2010, with each of the last three years (2018, 2019 and 2020) recording VSCS.

3.2 Case-studies

Four case studies of TCs which made landfall over the northeastern tip of Africa have been selected, to document the relationship between the tracks of these systems and the rainfall distribution. They are ordered here by increasing intensity.

- Deep depression ARB01/2013 (November 2013) :

This disturbance was first identified as a low pressure centre on 6 November 2013 near 6°N, 65°E (fig.3), then classified by the IMD as a tropical depression on 8 November 2013, while located 680 km east of Ras Binnah on the northeastern Somalian coast, moving westward. It slightly intensified on 9 November, with 3-mn sustained winds of 55 km/h, developed an eye feature, and was classified as a deep depression. It made landfall on 10 November at 8°30'N, north of Eyl in Puntland, northern Somalia. A large area of active convection was associated with the TC. Very high daily point rainfall estimates were obtained by IMERG along the track, from 199 mm to an unreliable 1196 mm on 9 November near the coast (fig.3, bottom), in conjunction with very low cloud top temperatures (-70 to -75°C, not shown). As the TC made landfall, very high rainfall estimates were still shown on 11 and 12 November over a large area covering northern Somalia. On 13-14 November, while the TC is no longer singularized, scattered but significant convective rains occurred from Djibouti to Central Somalia.

Rain-gauge data (fig.4) show that coastal rains associated with the disturbance started on 8 November, but the bulk of the rains fell on 11 November in arid Puntland (20 to 100 mm, and a peak of 139 mm at Eyl). The rains shifted westward on 12 November, with substantial rains (40-50 mm) still found on 13 November in western Somaliland. The accumulated rainfall during the TC lifetime (within 750 km of the TC center, fig.4) generally exceeds 100 mm in the east, and is more contrasted further west. However, if one adds the precipitation recorded in the following two days (fig.4, bottom right panel), rainfall amounts ranging from 49 to 144 mm are found in the inland part of western Somaliland. The coastal town of Berbera (55-yr MAR : 50 mm) even recorded 195 mm during this period. In Somalia, TC ARB01/2013 caused the death of 162 people, about 100,000 livestock losses and the destruction of over 1,000 houses according to official statistics (IFRC, 2013).

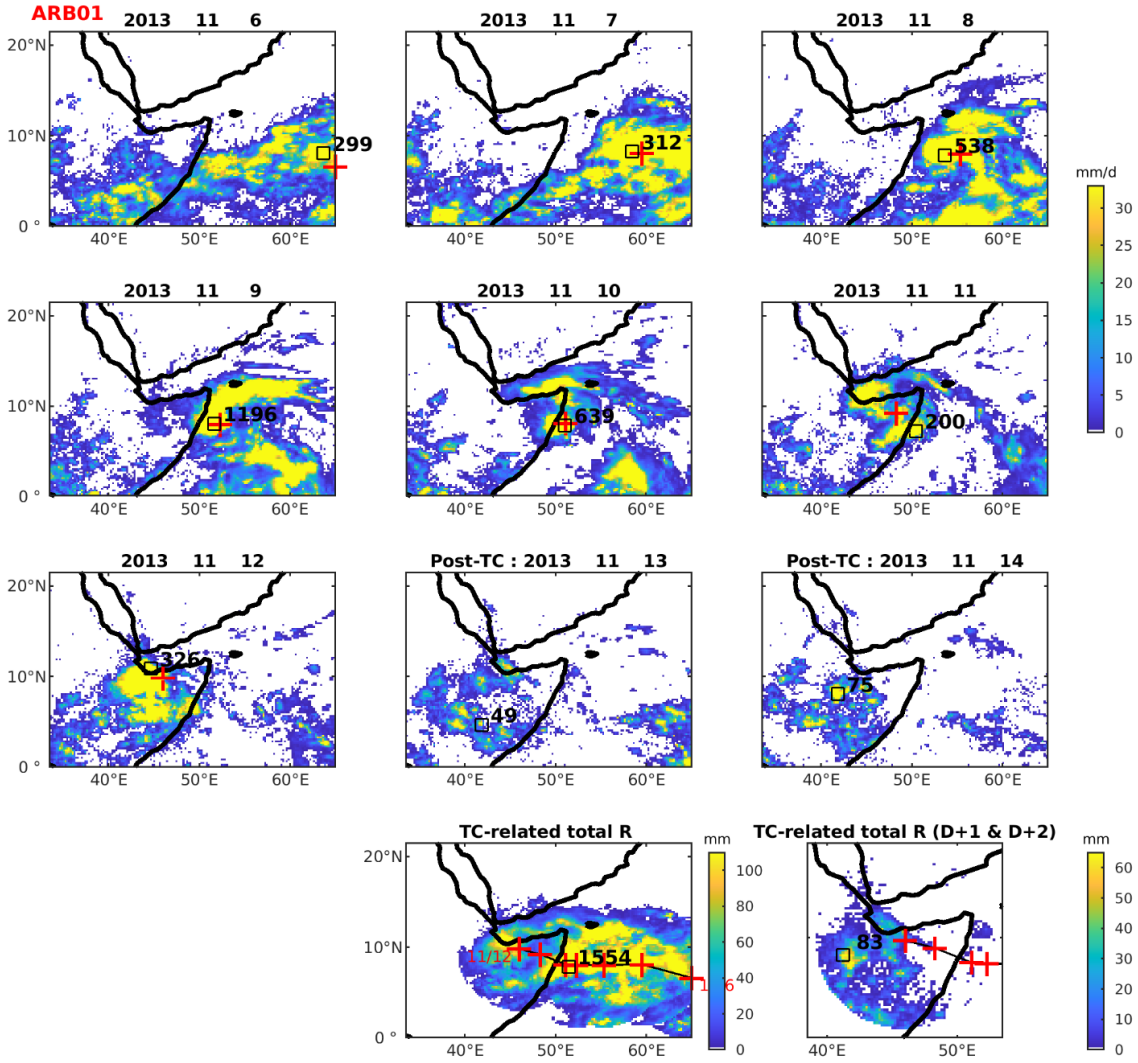

Figure 3 : IMERG daily rainfall during the lifetime of deep depression ARB01/2013 and in the two following days ("post-TC"). Bottom panels : accumulated rainfall amount associated with the TC (within 750 km of its center) during its lifetime (left) and in the two following days (right panel). Red crosses show the location of the TC center. Black figures : maximum rainfall amount within 750 km.

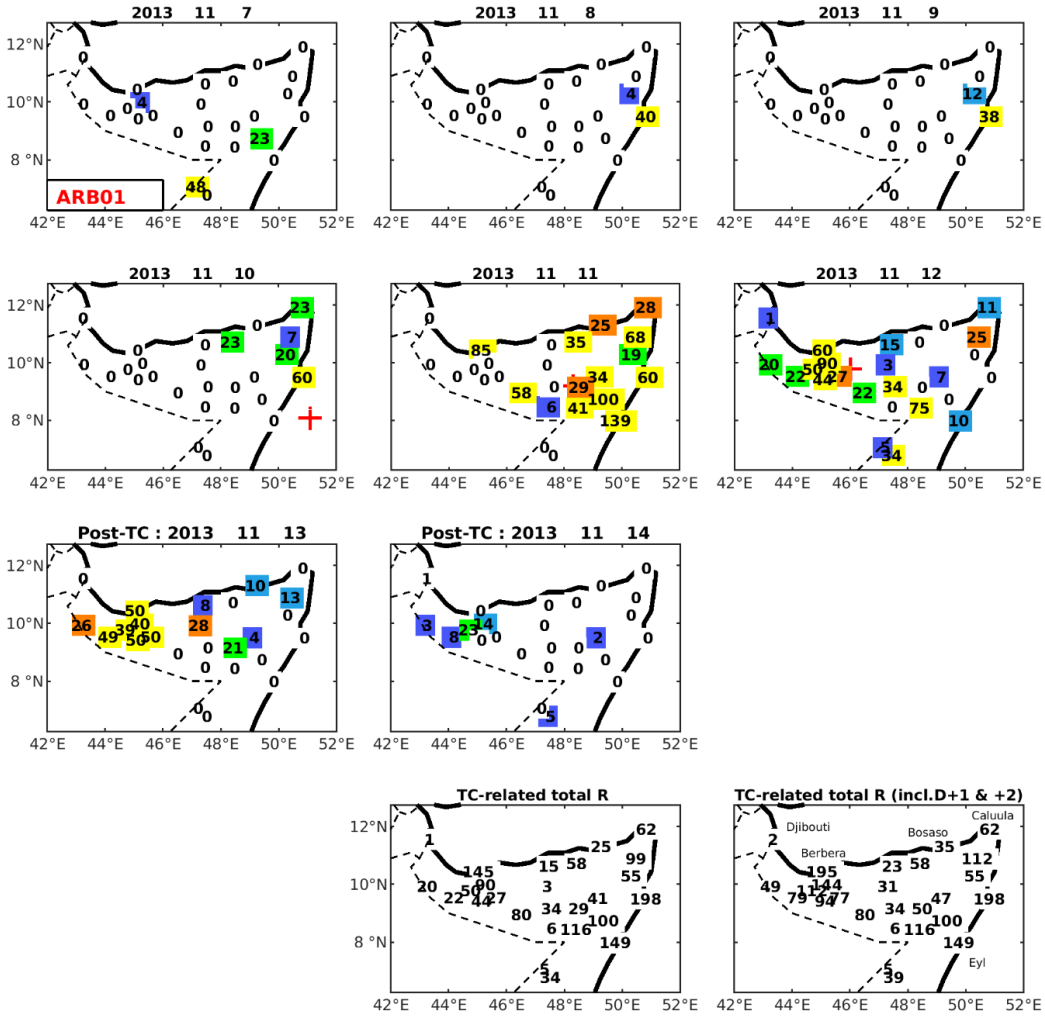

281

282 Figure 4 : Daily rainfall over Northern Somalia and Djibouti during the lifetime of deep depression
283 ARB01/2013 and in the two following days ("post-TC"). Bottom panels show the accumulated rainfall
284 amount associated with the TC (within 750 km of its center) during its lifetime (left) and including the
285 two following days (right panel).

286 - Cyclonic storm Sagar (May 2018)

287 According to the JTWC, this system began as a tropical depression on 15 May south of Socotra. It was
288 named Sagar after it reached the tropical storm stage (35 knots) near the entrance to the Gulf of
289 Aden on 16 May. The rains recorded off the eastern coast of Somalia on May 16-18 (fig.5, top left
290 panel) were mainly due to convective cells developing in the cloud bands at the southern edge of
291 Sagar. Proceeding towards the west-southwest, the storm gradually intensified to become a VSCS (65
292 knots) on May 18. The VIIRS image from 10:28 UTC in the visible spectrum indicates that Sagar was a
293 small diameter cyclone. On 19 May, returning to the severe cyclonic storm category (60 knots), Sagar
294 made landfall west of Berbera, Somaliland. The slow movement of the system and very cold cloud
295 top (-70°C to -80°C on Meteosat-8 images) largely explain the heavy rains observed in Somalia and

Djibouti from 18 to 20 May (fig.5, bottom panels). Substantial rains were also found on the following two days in eastern Ethiopia, associated with the overall atmospheric instability and Sagar remnants, causing landslides and flash floods destroying villages in the Sitti area.

Wadi Ambouli, which crosses Djibouti-city, overflowed and caused heavy damages, particularly on the right bank in the Boulaos neighbourhood. Around 20,000 people were affected in the Republic of Djibouti. Damage to transport infrastructure amounted to approximately 1.9 billion Djiboutian francs (US$10 million), with a similar figure for the sanitation system (Cherel et al. 2020). At least 53 victims were numbered in northern Somalia, particularly in western Somaliland, herds were swept away, and many boats were destroyed in the ports of Puntland.

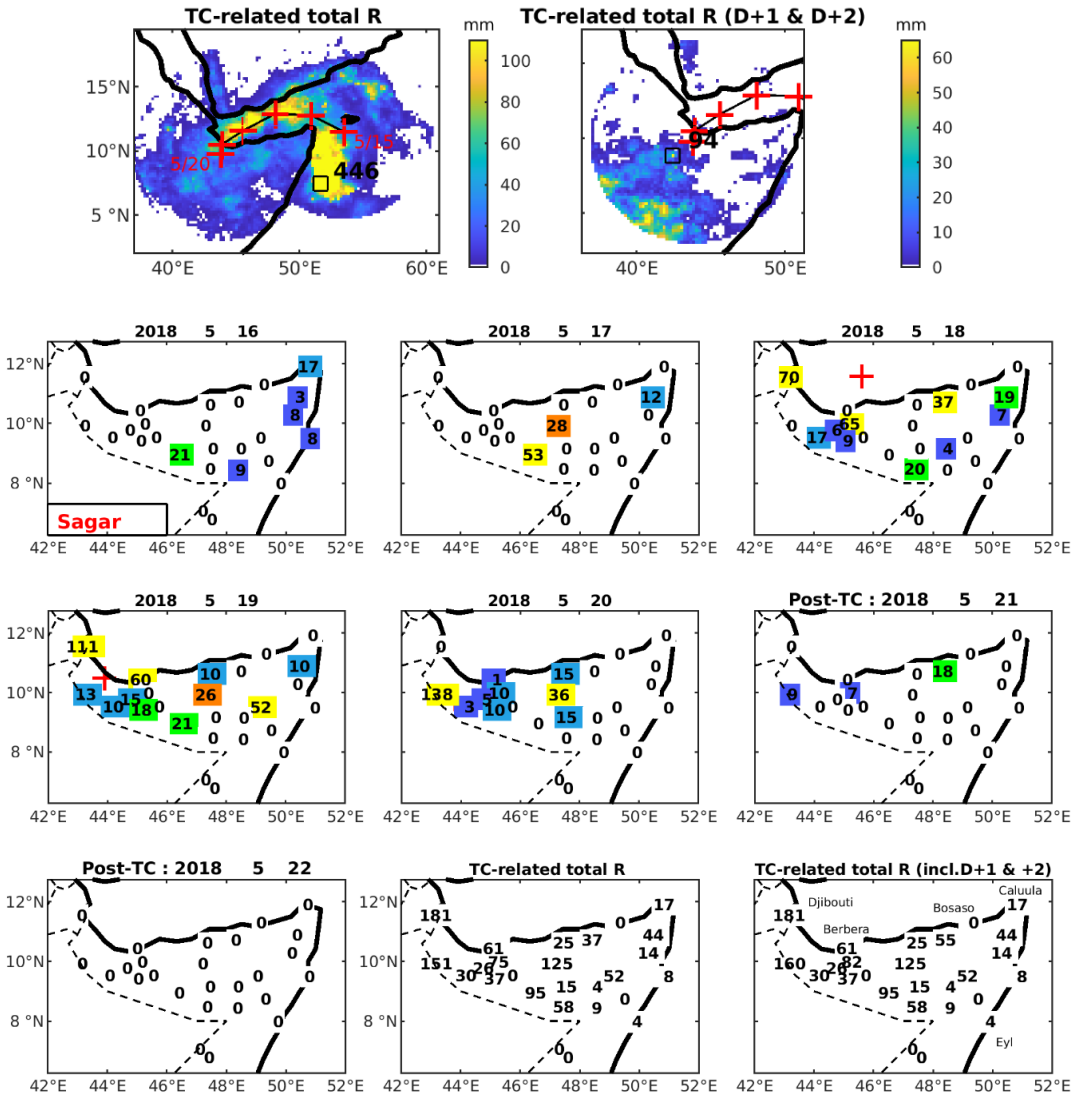

Figure 5 : Rainfall associated with TC Sagar. Top panels : accumulated IMERG rainfall during Sagar lifetime (15-20 May, top left) and in the two following days (21-22 May, top right). Red crosses show the location of the TC center, with indication of the first and last dates of its lifetime. Black squares

indicate the maximum accumulated rainfall amount (mm) within the 750 kms of the center. Bottom panels : daily rainfall over Northern Somalia and Djibouti and in the two following days ("post-TC").

- VSCS Gati (November 2020)

Gati is a recent example of a VSCS which showed an explosive intensification from a low pressure area located in the central Arabian Sea on 20 November 2020. Moving westwards (fig.6), it made landfall near Hafun in northeastern Somalia on 22 November as a VSCS. Gati quickly weakened as it crossed land, with a last warning issued on 23 November over the gulf of Aden. It resulted in maximum daily rainfall exceeding 100-200 mm every day from 20 to 23 November over the WAS, and in northeastern Somalia (fig.7) several stations recorded daily rains over 70 mm on 22 and 23 November (e.g., at the hyper-arid station of Bosaso, 128 mm on 23 November, i.e. 780% of the 51-yr MAR). Rainfall was lower further west, though an IMERG estimate of 180 mm is still noted in the Gulf of Aden on 24 November, and 65 mm recorded at Berbera on 25 November. Weaker rains were observed in Djibouti, but remnants of the storm brought heavy local rains on 25-26 November in eastern Ethiopia. 42,000 people were displaced in Bari region, Puntland, Northeastern Somalia, with extensive damages due to flash floods, coastal submersion and winds (OCHA, 2020).

Although Gati had a trajectory roughly similar to that of Sagar, the heavy rains were felt more in the eastern than in the western part of its track. A detailed meteorological analysis is again out of scope, but the early landfall of Gati explained its fast weakening, hence the weaker rains in Western Somaliland and Djibouti. The more curvilinear path of Sagar, over the very warm Gulf of Aden (XBT soundings indicated that water temperature exceeded 27°C up to a depth of at least 29m, not shown), provided a considerable heat flux which was sufficient to feed Sagar, despite its relatively slow motion.

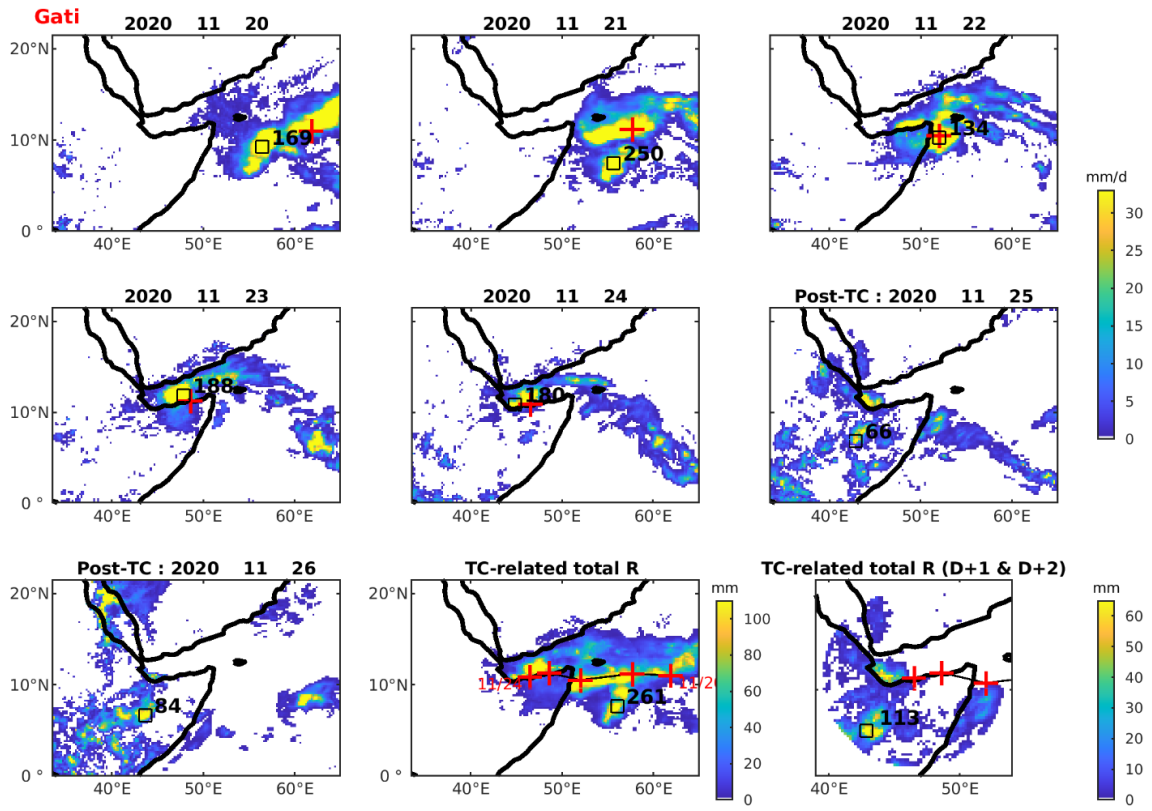

331

332 Figure 6 : same as figure 3 but for VSCS Gati

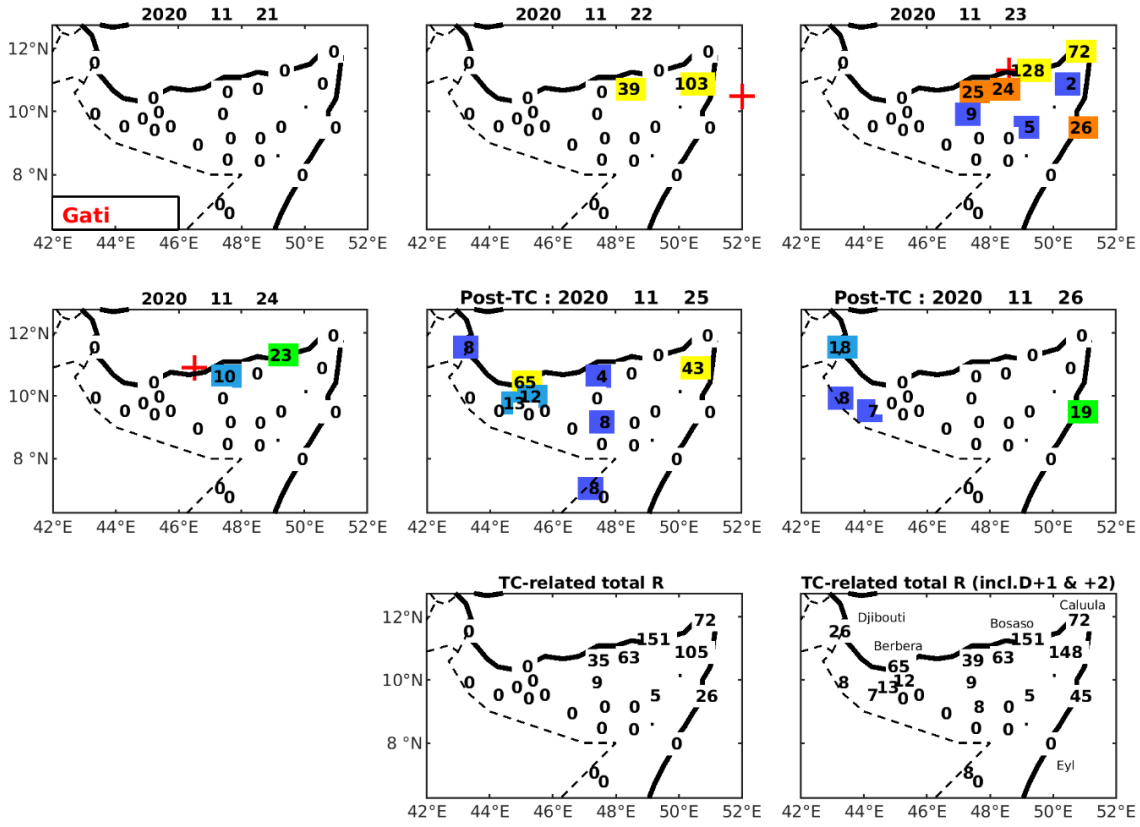

333

334 Figure 7 : same as figure 4 but for VSCS Gati.

- VSCS 12A (October 1972) :

Although rainfall maps are not available for this disturbance, since it predates the satellite era, it is an interesting case typical of the probable underreporting of some TC-related rainfall in the region, in this case due to incomplete TC tracks before 1982. Storm 12A originated from the southern Arabian Sea, moving northwestward to cross Socotra Island. It was classified as a VSCS (64-82 knots) just before its landfall over Socotra, then continued westwards while weakening. According to IBTrACS, this storm was last located at 12.2°N, 50.8°E, i.e. 20 km north of Caluula, near Cape Guardafui, on 25 October 12:00 (with perfect agreement between the three IBTrACS sources). Yet the October 1972 monthly weather report in Djibouti (Résumé Mensuel du Temps, 1972) indicated that the storm, after entering the Gulf of Aden on 25 October at a speed of 5-6 knots, further penetrated westward with increased velocity (25-30 knots) and reached Djibouti in the morning of 27 October. Wind gusts of 36 knots were reported at Djibouti-Airport, 45 knots at Arta 40 km westwards. The track of this TC, along the Gulf of Aden, is therefore closer to Sagar in 2018 than Gati or ARB01. The relatively small size of the tropical systems which enter the Gulf of Aden, like storm 12A, may, before the satellite era, have resulted in their underreporting.

Exceptionally high rains fell in the Djibouti area (201 mm at Djibouti-Airport on 27 October, 118% of the MAR), over the Gouda mountains (at Randa, 133 mm on the same day, 94 mm on 28 October) and at the usually very dry northern coastal station of Obock (105 mm on 27-28 October, compared to a MAR of only 73 mm). Rainfall quickly decreased further west, with only 2 mm at Dikhil and no rain at all at As Eyla. There is no daily data available from the northern coast of Somalia, while heavy rains fell further south in Central Somalia, but unlikely to be directly TC-related. Stations located over the Northern Somalia Highlands, though close to the Gulf of Aden, reported only little rainfall (Hargeysa 6 mm on 28-29 October 1972), suggesting that the storm was of moderate size at this stage. There is only scanty information to assess the human losses and damages resulting from the storm. In Djibouti 60 people were reported dead and 5000 homeless. In Somalia, a third of the coastal palm groves in northeastern Somalia were destroyed by the storm, with long-lasting effects on spring discharges due to landslides (Chazée, 2017).

Overall, several inferences can be made from these four case studies. First, although defining the exact zone of TC-related rainfall is uneasy, it is clear (e.g., fig.3) that on several days this area extends beyond 500 km from the TC center. Second, in the two days following the reported termination date of the system, substantial rainfall, especially over land where the disturbance does not meet all the criteria to qualify as a tropical storm, is associated with remnants of the TC. Land rainfall related to the TC matches reasonably well between IMERG and rain-gauge data, though a detailed comparison is out of

scope. Lastly, intense rainfall, with little relationship to the storm category, can be observed at arid locations. For instance, in northeastern Somalia, rainfall from deep depression ARB01/2013 (35 to 198 mm) often equals or exceeds MAR, which is as little as 15 to 200 mm. Over the ocean, even higher rainfall amounts are found in IMERG, but they are highly localized.

3.3 Statistics of rainfall associated with TC occurrence

This section aims to produce a statistical analysis of TC-related rainfall, over the period 2000-2020 for which cyclone data are very reliable and different sources of rainfall data are available. Rainfall on TC-days is plotted as a function of the distance to the TC center, for PERSIANN and IMERG (figure 8). Both plots clearly show an exponential decay from the center. However, close to the center, rainfall is more intense in IMERG (83 mm at 0-20 km) than in PERSIANN (41 mm). This is partly due to the higher spatial resolution of IMERG, which better resolves very intense but highly localised downpours, and to the algorithm and input data used to estimating rainfall, which include microwave and radar data in IMERG. When screening for VSCS only (turquoise lines on fig.9), even higher rainfall is noted close to the TC center. Gaona et al. (2018) showed the added value of IMERG in depicting rainfall intensities close to the TC center.

After a strong decrease of rainfall amounts with increasing distance, the slope markedly reduces beyond 400 to 500 km, before gradually flattening out. The distance from which rainfall decreases becomes negligible and a mere straight line is around 600 km for IMERG and 700 km for PERSIANN. Given that the boxplot height is smallest around 750 km in PERSIANN, we retain this distance as a conservative threshold below which rainfall is considered as TC-related (and referred to as such hereafter). This distance is greater than in most previous studies (500 km), but it is justified by the fact the daily time-scale used in this study involves some propagation of the TC in a 24-hr period. Additionally, a cursory look at individual cyclones confirmed that a 500 km radius would exclude, in some cases, areas of convective activity which are clearly part of the disturbance. Note that for VSCS only, the drop to very low rainfall occurs at a slightly shorter distance, despite the much higher core intensities, suggesting more compact disturbances.

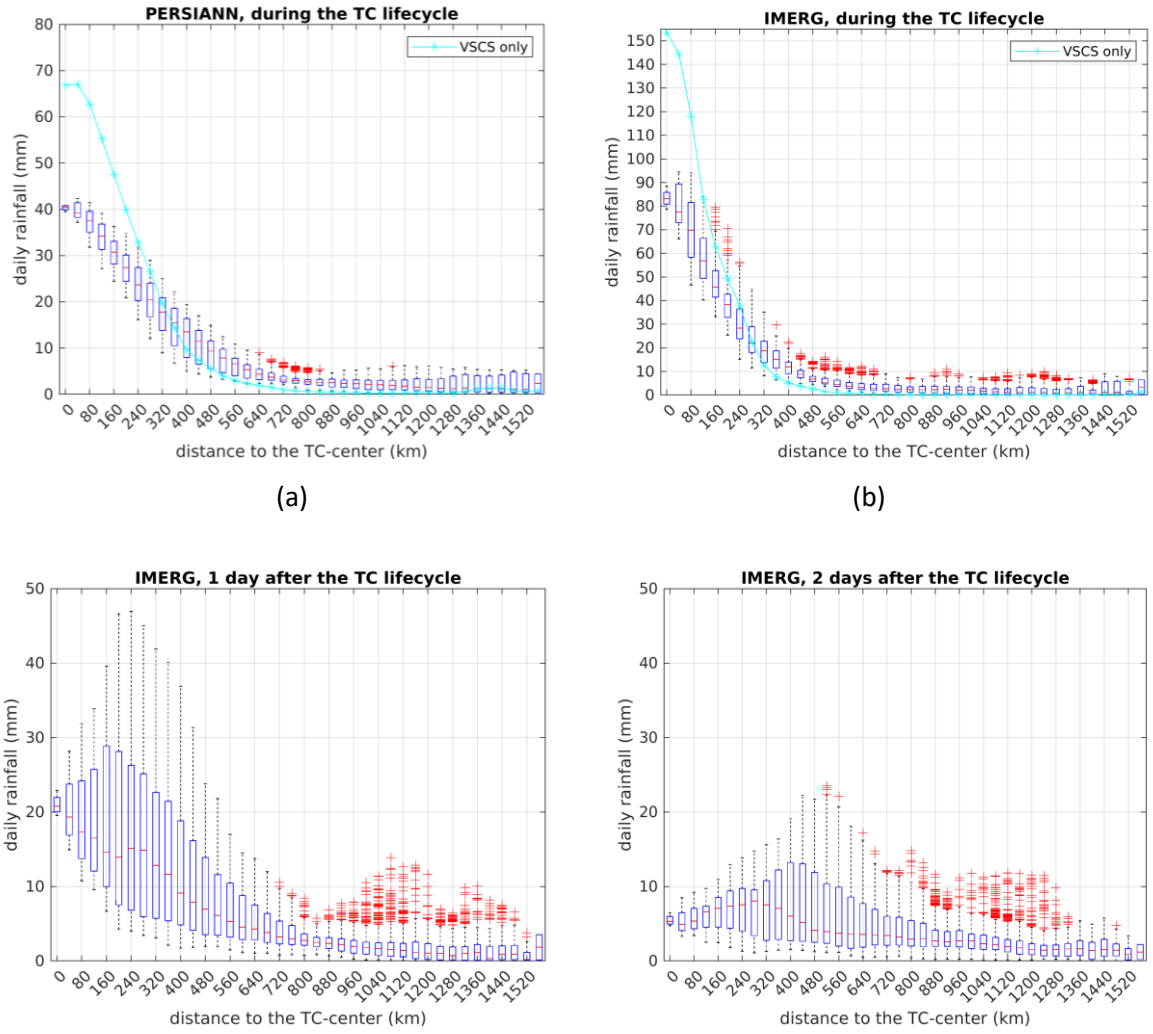

Figure 8 : Boxplots of mean daily rainfall observed on TC-days over the WAS, as a function of the distance to the TC center, using PERSIANN (a) and IMERG (b) data for 2000-2020. Bottom row : mean IMERG daily rainfall a day (c) and two days (d) after the end of the TC lifecycle (the TC center refers to its last known location). The spread of the boxplots refers to spatial variations (i.e., in the mean rainfall among the pixels located in each distance bin). On panels (a) and (b), turquoise lines and stars show the median rainfall observed on VSCS only. Note the different vertical scales.

As suggested by the above case-studies, TC-related rainfall does not necessarily stop as soon as the TC is no longer defined. Figure 8 shows rainfall one (panel c) and two days (panel d) after the TC lifecycle. On day+1, heavy rains (median of 21 mm/day) are still found within 20 km of the last known TC location. Between 40 and 400 km, although the elongated boxplots denote a diversity of patterns, substantial rains (medians from 9 to 19 mm/day) reflect active remnants of the storm. On day+2, rainfall markedly decreases, but rains above 5 mm/day (again with a high dispersion) are found up to 400 km, with a median peaking at 8 mm at 280 km because of the shift of the storm remnants. This

suggests that post-TC rainfall cannot be neglected. Hence, in the following, TC-related rainfall will be considered as the accumulated rainfall during the entire TC lifetime plus the following two days.

Mean rainfall on TC days and non-TC days is plotted for MJ and SOND (figure 9). TCs bring substantial rains in the northwestern Arabian Sea, an otherwise relatively dry area in both seasons. Over the sea around Socotra and further to the north-east, intensities between 4 and 10 mm/day are recorded on TC days, while mean rainfall on other days of the same seasons is generally below 1.5 mm/day. The patterns are quite similar for the two seasons, although more noisy for AMJ because TCs are less frequent. Near and along the coasts of northern Somalia, southern Yemen, southern Oman and in the Gulf of Aden, TC-related intensities are lower but in a context of even more arid conditions (<0.5 mm/day on non-TC days). This mostly reflects the smaller number of TCs reaching these areas. Over a broad area covering the northwestern Arabian Sea and nearby regions, the mean rainfall intensity is statistically higher (t-test, $p<0.05$) on TC-days than during the same calendar days for years with no TCs (i.e., same day climatology: Fig. 9b & d). Interestingly, some significant rainfall anomalies are also found remotely from the WAS. Over central Ethiopia, localised drier than normal conditions (white circles) are found in SOND when a TC occurs in the WAS. By contrast, more rains than normal occur over Western Kenya (36-38°E, 2°S-5°N) in both seasons. This points to the distant effect of TCs, which will not be addressed here, but was already discussed for Southern Hemisphere cyclones (Shanko and Camberlin, 1998 ; Finney et al., 2020 ; Kebacho, 2022).

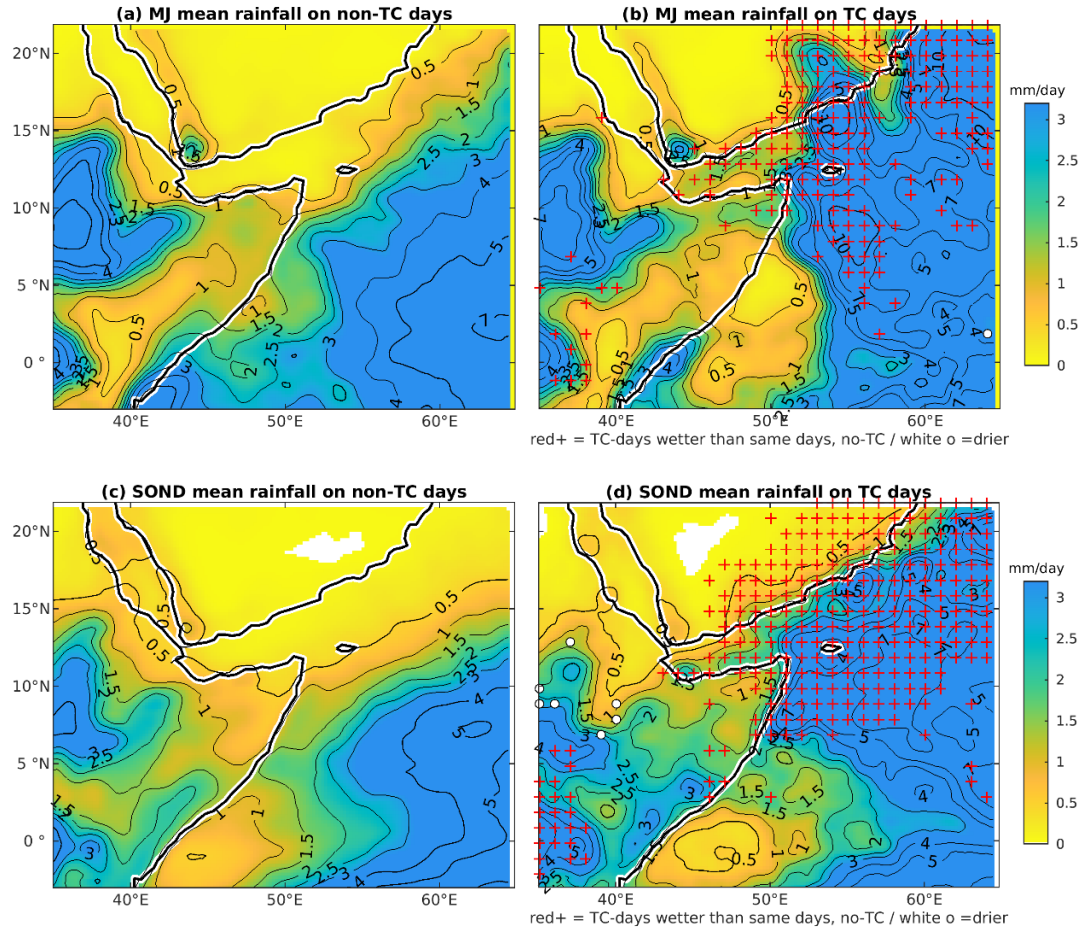

Figure 9: Rainfall (mm/day) on non-TC days (left panels) and TC days (right panels) for May-June (a,b) and September-December (c, d), based on IMERG data (2000-2020). Red plus signs (white circles) indicate grid-points where rainfall on TC-days is significantly higher (lower) ($p<0.05$) than that recorded on the same calendar days but with no-TC.

TC-related rainfall makes a very high contribution to seasonal rainfall over the Arabian Sea northeast of Cape Guardafui (fig.10). Over the northwestern Arabian Sea and Gulf of Aden, contributions reach 30 to 50% along a belt running from the Gulf of Aden to Socotra island and the Yemen and Oman coasts. Contributions are more variable in MJ than SOND due to the small number of disturbances and their haphazard tracks. Values locally exceed 60% near the coasts, including inland southern Arabia near the border between Oman and Yemen. High contributions are also found at the northeastern tip of Somalia (30-50%), quickly decreasing inland. On an annual basis (not shown), contributions exceed 30%, and even more than 50% over some areas according to PERSIANN. These values are quite remarkable given the relatively low occurrence of TCs in this basin. They are higher than those published in Prat and Nelson (2013) for the Arabian Sea, for several reasons like the different data set they used (TRMM), methodology, and their period of study (1998-2009) which does not include the recent very active years. These are among the highest values in the world. Among the cyclonic regions examined by Khouakhi et al. (2017), such high contributions are reached over only a few coastal areas

in the world, like Northwestern Australia, Baja California, the northern Philippines and Hainan island in China, although their study did not consider oceanic areas.

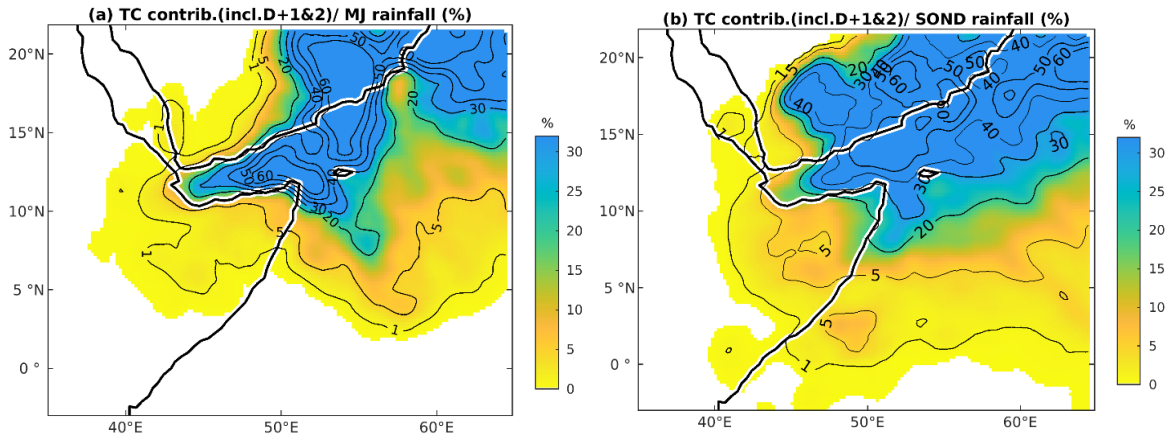

Figure 10: Percentage contribution of TC-related rainfall to mean seasonal rainfall (IMERG data, 2000-2020), for MJ (a) and SOND (b). TC-related rainfall refers to rainfall within 750 km of the TC center, during its lifetime or in the next two days

Rain-gauge records confirm that over Northern Somalia the contribution of TC-related rainfall is often moderate, though it strongly increases along the coasts (fig.11). In MJ (fig.11a), it is below 10% inland, but much higher along the shores of the Gulf of Aden, in agreement with the higher contributions found over the sea in IMERG. In the western part of the Gulf, a high value (53%) is obtained at Djibouti, much higher than IMERG (10%). In agreement with IMERG, and with the exception of the Gulf of Aden, SOND contributions (fig.11b) are generally higher than in MJ, due to a larger number of TCs. A broad east to west decrease is noted, which highlights the dominant westward tracks (figure 2). However, arid stations along the Gulf of Aden get SOND contributions as high as 46% (Bosaso) and 47% (Berbera). Given the small number of TCs making landfall over the GHA, these are exceptionally high contributions.

The importance of TCs on rainfall is further underlined by focusing on intense rainfall events. Rain days recording more than 30 mm (IMERG data) are examined to find out how much TCs were contributing to these events. Over most of the Horn of Africa, the northern Arabian Sea, and moreover the southern Arabian Peninsula, the number of intense rainfall days is small (frequency <1%, i.e. less than 0.6 day.year^{-1} in MJ and 1.2 in SOND, not shown). Conspicuously, a large share of these days (>40%, fig. 11e-f) is brought by TCs in the northwestern Arabian Sea and the Gulf of Aden, and in northeastern Somalia in SOND. This share even exceeds 60% over a belt extending from NE to SW along and offshore the Arabian Coast.

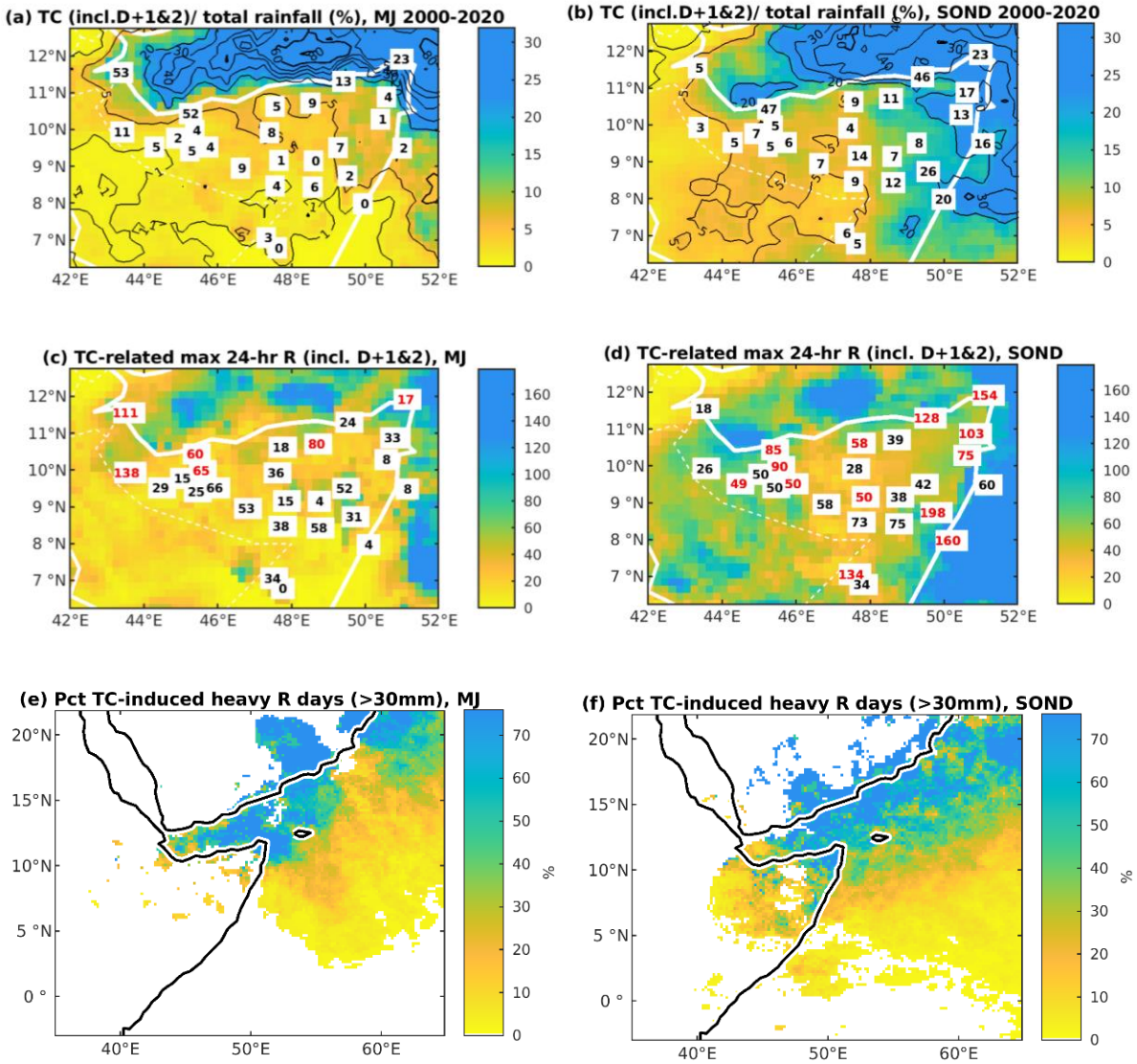

475

476

477 Fig. 11: Rainfall statistics associated with TCs over Northern Somalia, Djibouti and neighbouring
478 areas, based on rain-gauge data (figures) and IMERG (shadings), for MJ (left panels) and SOND (right
479 panels). Percentage contribution of TC-related rainfall to mean seasonal rainfall (a,b) ; maximum TC-
480 related 24-hr rainfall in mm (c,d) ; percent of days above 30 mm which are TC-induced (e,f), 2000-
481 2020. In panels c,d, a value in red indicates that it is the highest 24-hr amount recorded at a given
482 station in the respective season. TC-related rainfall refers to rainfall within 750 km of the TC center,
483 during its lifetime or in the two following days.

484 Rain-gauge data for northern Somalia and Djibouti confirm that in SOND at many stations the highest
485 24-hr rainfall is attributed to a TC (figure 11d). In general, the maximum TC-related 24-hr rainfall is
486 over 50 mm in this season, reaching values beyond 100 mm in most of the eastern stations. This is
487 broadly in line with IMERG values. In MJ (figure 11c), the highest TC-related 24-hr rainfall amounts are
488 lower over the continent, and clearly more patchy (over the sea as well) as a result of fewer TCs.

Interestingly, high values are nevertheless obtained in the north-west (60 mm at Berbera, 111 mm at Djibouti and 138 mm at Borama). Very intense rains are also associated with TC landfall over Oman (in Salalah for example, the absolute maximum rainfall measured during 1990-2020, 238.8 mm, was associated with the passage of cyclone Mekunu on May 25, 2018), but TC occurrence in this country is more thoroughly discussed in Pedgley (1969) and Al-Manji et al. (2021). Though IMERG also shows high values in the Gulf of Aden itself, near the coast satellite estimates are often lower than the observed contributions, because occasional very heavy precipitation along the coast are not always adequately resolved by the gridded products. Such an underestimation of coastal intense precipitation in gridded products is found in other parts of Africa (e.g., the Guinea Coast ; Kpanou et al. 2021).

On the whole, despite the high expected variability associated with extreme point rainfall, relatively consistent patterns emerge in the northeastern Horn of Africa, which confirm the strong role of TCs on intense rainfall along the northern and eastern coasts in SOND, around the gulf of Aden in MJ, as well as a substantial contribution inland but in SOND only.

3.4 Trends in rainfall and TC-related rainfall

Annual rainfall trends are first analysed over the period 2000-2020 (fig.12a). For IMERG data, positive trends largely dominate, with the largest values (+5 to 10 mm/yr) over inland Somalia and much of the WAS and Western Indian Ocean, although pockets of negative trends are found further offshore, notably around 5°N-60°E. There is some uncertainty about these negative trends, as PERSIANN data, over the same period, display positive trends even far offshore (not shown). Weaker but statistically significant positive trends ($p<0.05$) are found over the Gulf of Aden. When focusing on TC-related rainfall only (fig.12b), there are widespread positive trends for both IMERG and PERSIANN data, though their magnitude is smaller, except over the Arabian Sea near 10-12°N where trends over +5mm/yr are noticed. The latter are statistically significant, as well as the (weaker) positive trends which are found over the Gulf of Aden and neighbouring areas (Djibouti, Yemen, northwestern Somalia). The contribution of TCs to total rainfall shows significant positive trends over the same regions, with a 21-yr increase ranging from 20 to 35 points over the areas where the change is the largest, i.e. part of the WAS, the coasts of Oman and Yemen, and the Gulf of Aden (fig. 12d). When removing TC-related rainfall from total amounts (fig.12c), trend patterns become close to zero or weakly positive in the northern part of the region, suggesting that much of the recent increased rainfall is due to the more frequent (and more intense) TCs. Over the African continent, apart from some coastal areas, there is little difference between the total and non-TC-related rainfall trends, despite the trend associated with TCs being significant, because TCs only contribute to a minor fraction of the rains.

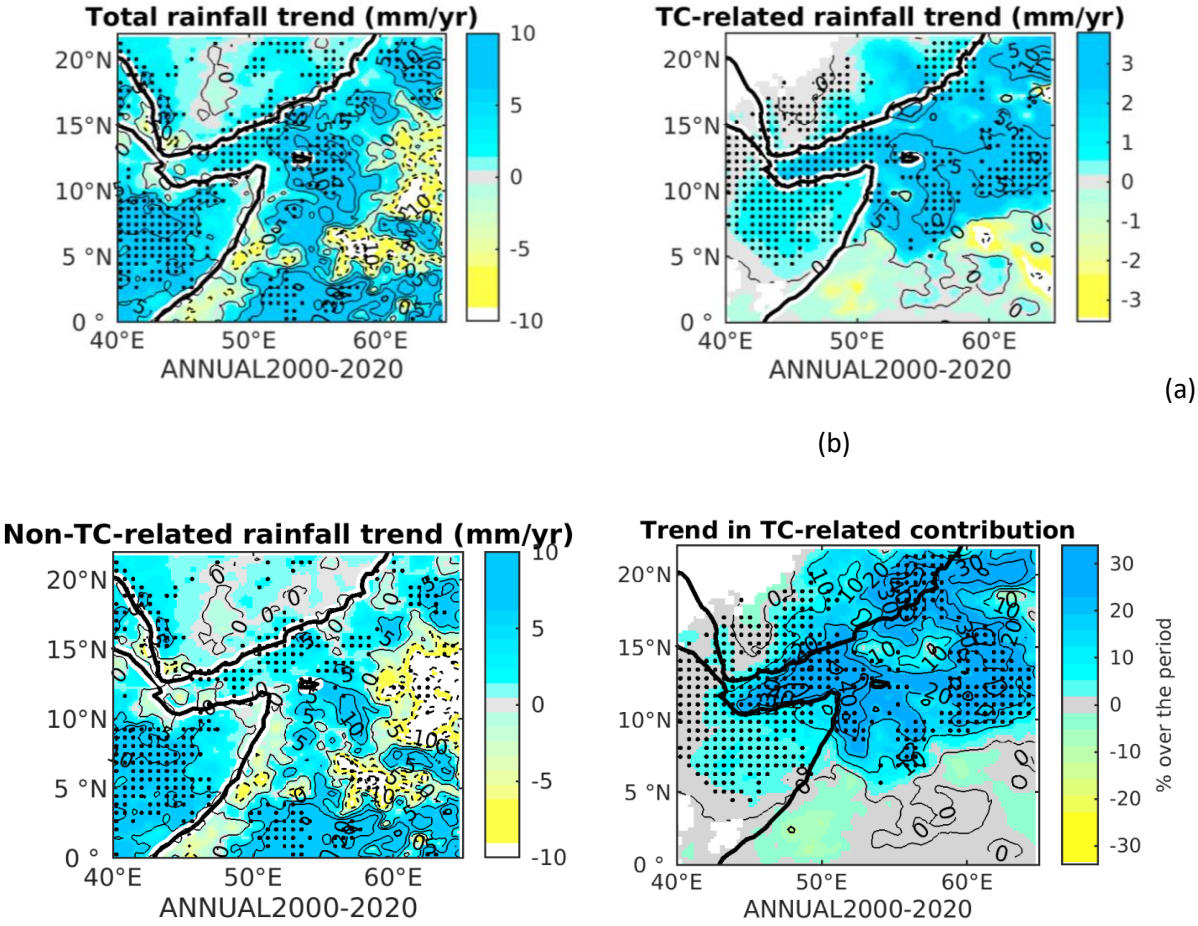

(a) (b) (c) (d)

Figure 12 : Trends in annual rainfall, IMERG, 2000-2020. Total rainfall (a), TC-related rainfall (b), non-TC related rainfall (c) and contribution of TC-related rainfall to the rainfall total (d). Dots indicate significant trends ($p<0.05$) according to the Mann-Kendall test statistic.

A seasonal analysis (not shown) indicates that these trends are found during both MJ and SOND, although they are stronger and spatially more consistent for SOND. During this season, a very strong and significant ($p<0.05$) increase in the TC contribution is noted between 10 and 17°N. In the 21-yr period 2000-2020, the contribution of TCs to SOND rainfall amounts increased by 30 to 50% in the Gulf of Aden and the Arabian Sea east of Socotra island. A similar rise is found from the Gulf of Aden to southern Oman in MJ, but it is more patchy and seldom significant, due to the rare occurrence of TCs in the pre-monsoon season, resulting in many years (even in the more recent period) with nil TC-related rainfall.

For a better appraisal of trends over the Gulf of Aden and its shores, a regional rainfall index (location shown on figure 1) is extracted and plotted in figure 13. For PERSIANN, the time-series were extended

to include the full period from 1990 to 2020. Total rainfall shows a weak positive long-term trend (+0.44 mm/yr from 1990 to 2020, i.e. +8% in 31 years). TCs strongly contribute to this trend, as shown by the conspicuous increase in TC-related rainfall (+0.67 mm/yr fig.13b). If one deducts TC-related rainfall from the annual rainfall, the trend becomes slightly negative (-0.23 mm/yr, Ii.e. about -4% in 31 years). The contrast between the almost absence of any TC in the sub-period 1990-2007 and the relatively frequent TCs in the sub-period 2008-2020 is noteworthy. Besides the higher frequency of TCs, rainfall associated with each TC tends to significantly increase between 1990 and 2020 (Mann-Kendall tau, $p<0.01$, not shown).

Over the period common to the two data sets, IMERG data show a relatively good agreement with PERSIANN in the interannual variations of total and TC-related rainfall. Over this period (2000-2020), the increase in TC-related rains is strong (+0.99 mm/yr in IMERG, fig.13b). This trend also strongly contributes to the overall rainfall trend (+1.40 mm/yr), while the non-TC-related trend is weaker. As described above, there is a marked increase in the contribution of TCs to total rainfall, which was close to zero before 2007 and reached 9.3% in 2008-2020.

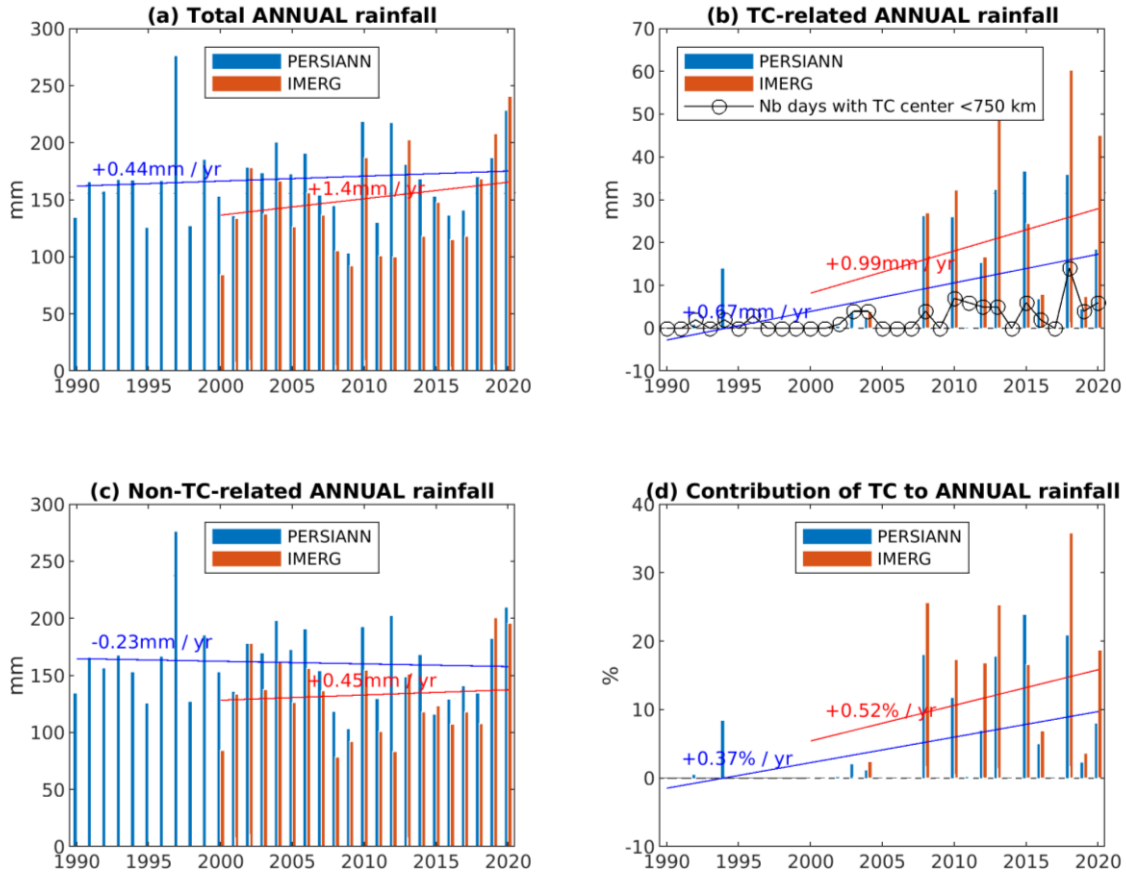

Figure 13 : Annual rainfall variations and trends over the Gulf of Aden and its shores (44-50°E, 10-14°N): total rainfall (a), TC-related rainfall (b), non-TC-related rainfall (c), and contribution of TCs to total rainfall (d).

The increase concerns both cyclonic seasons, although pre-monsoon TCs are still a rarity in the Gulf of Aden (fig.14). The increase in TC-related rainfall boosts the May rainfall peak in the second sub-period, and strongly contributes to alleviate the decrease which would have otherwise been found in October-December. At that time, TCs have a strong effect on rainfall amounts in the arid environment of the Gulf of Aden. In the sub-period 2008-2020, the increase in the frequency of TCs makes the contribution of TCs to total October-December rainfall reach 32.4%, from 2.5% in 1990-2007. These statistics are based on a sufficient number of events to be meaningful: during this season, from 2008 to 2020, 17 TCs hit the Gulf of Aden or approached it (within the 750 km radius), as against only 4 in the previous sub-period.

The on-and-off TC activity in the Gulf of Aden (and the Arabian Sea in general) is a conspicuous feature (fig.13). Roy Chowdhury et al. (2020) showed that the positive Indian Ocean Dipole (IOD) event that occurred in 2015 stimulated the development of the dual TCs Chapala and Megh in the WAS in October-November, through a warmer than normal western Indian Ocean and lower sea-level pressure. Similar conclusions were reached by Akhila et al. (2022), who studied cyclones Kyarr and Maha in 2019, a positive IOD year. However, Yuan and Cao (2013) and Sattar and Cheung (2019) got more ambiguous results on the systematic role of the IOD on Arabian Sea cyclones.

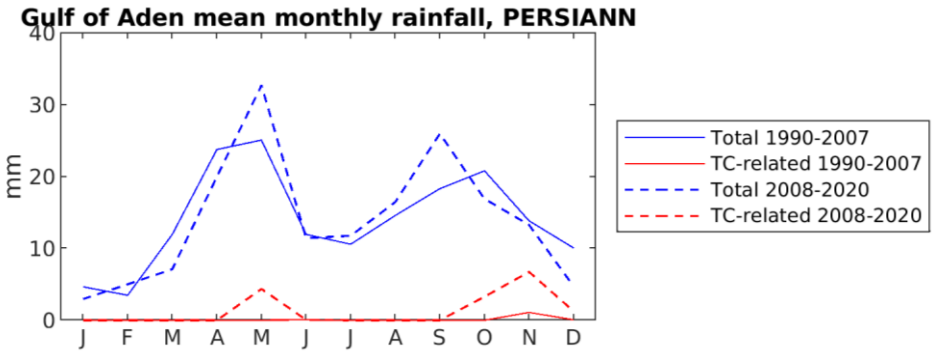

Figure 14: Mean monthly rainfall over the Gulf of Aden area (PERSIANN data ; IMERG data not shown because of the small number of years available in the first sub-period), for 1990-2007 (solid lines) and 2008-2020 (dashed). Blue lines: total rainfall; red lines: TC-related rainfall.

3.5 Regional changes contributing to the TC increase

The changes in the oceanic and atmospheric conditions which may have accounted for the recent increase in the number of TCs or severe storms in the Arabian Sea have been partly documented by Deo et al. (2011), Deshpande et al. (2021) and Tiwari et al. (2022). This issue is further documented here, separately for the two cyclonic seasons, and by taking into account the detection of a change-point (in 2010) in the number of TC days in the WAS (figure 2). Differences between the sub-periods

1990-2009 and 2010-2020 are plotted in figure 15 using ERA5 reanalysis data (similar results are obtained using the NCEP-NCAR reanalysis).

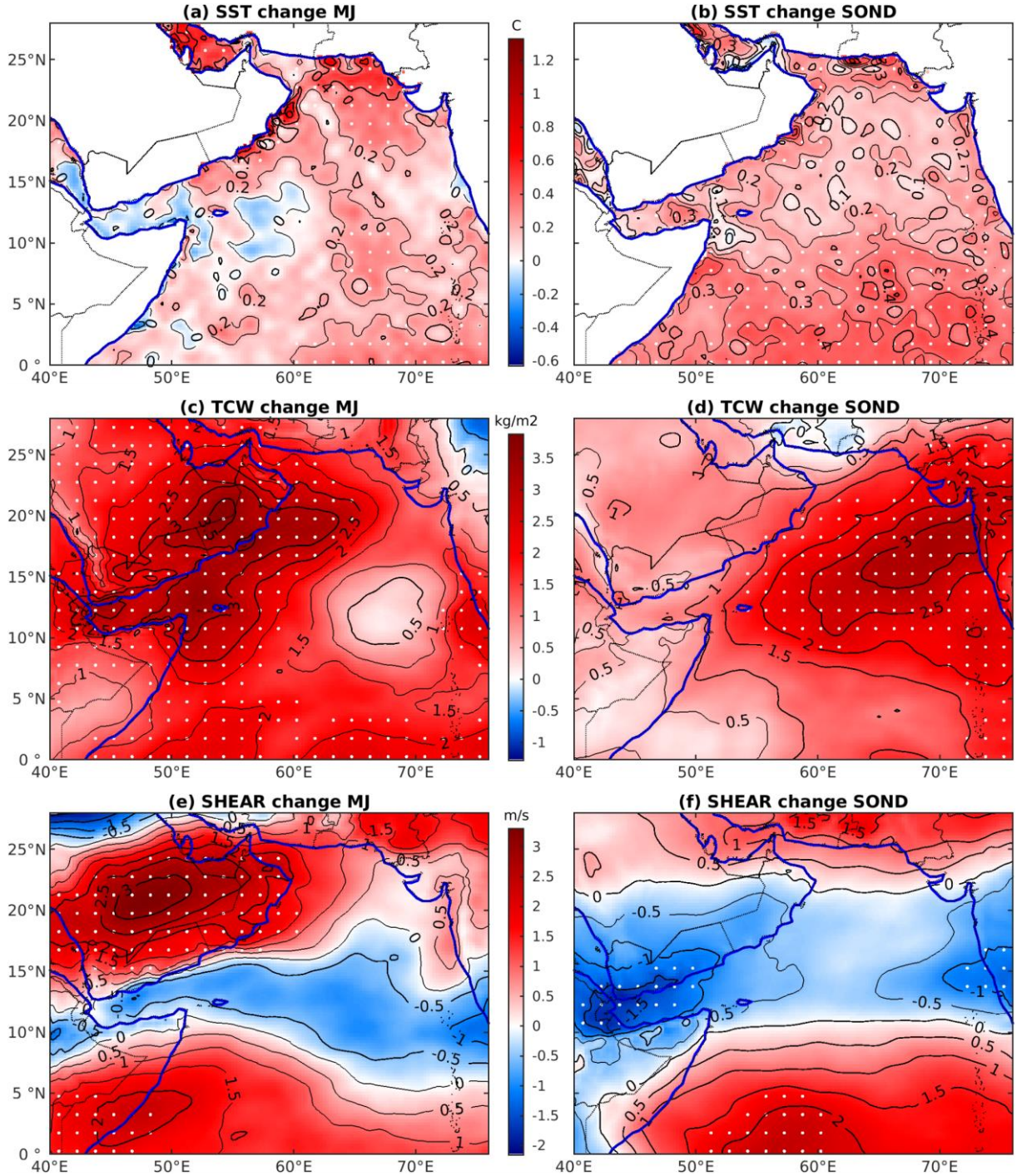

Figure 15: Changes in sea-surface temperature (a-b), total column water (c-d) and vertical wind shear (e-f) from 1990-2009 to 2010-2020, for the MJ and SOND seasons (ERA5 data). White dots indicate statistically significant changes (t-test, $p<0.05$). The change in wind shear is computed as the magnitude change between 200 and 850 hPa wind vectors (Pillay and Fitchett 2021).

The tripling of the number of days with TCs between 1990-2009 (4 days per year) and 2010-2020 (13 days per) in the WAS is found to be associated with three features favourable to TC activity :

(1) a decrease in vertical wind shear between 200 hPa and 850 hPa in a belt running from India to the Gulf of Aden, in both seasons (the decrease is significant in SOND only ; fig.15e-f)

(2) a sharp increase in relative humidity in the mid-troposphere (700 to 500 hPa) and of total column water (fig.15 c-d), mainly in the northwestern part of the region in MJ and in the eastern part in SOND

(3) an increase in sea surface temperature (SST, fig. 15a-b), which is more widespread in SOND than in MJ (for the latter, the Gulf of Aden and neighbouring areas do not show any clear warming)

The main source region of TCs, i.e. the southeastern Arabian Sea, displays the strongest sea surface warming, which may account for more favourable conditions for TC genesis, given that other factors in the same region (wind shear, atmospheric moisture) also tend to be more favourable. In the WAS, it is the strong increase in total column water vapour, in MJ, and the reduced wind shear, in SOND, which seem to constitute the key triggers, likely enabling existing systems to have a longer lifetime or to intensify. Part of these changes denote the effect of decadal-scale variability, since during the pre-monsoon vertical wind shear in the WAS for the decade 2000-09 was higher than in 1990-99. This impacted the lower cyclone activity during part of the first sub-period. Deshpande et al. (2021) also pointed to an increase of TC genesis at lower latitudes, which due to the dominant easterlies across the Somalia and Yemen shorelines, contribute to the increased number of WAS cyclones during the most recent period (examples of 03A in November 2013, Sagar in 2018, Gati in 2020). It is unclear whether these trends denote changes in TC activity due to anthropogenic climate change, but the Arabian Sea is one of the ocean basins where models most consistently project a forthcoming increase in intense TCs (Murakami et al. 2013; Knutson et al., 2015 ; Bell et al. 2020).

4. Conclusions

The northwestern Arabian Sea and adjacent land areas are among the few regions of the world where tropical cyclones occur in an arid context. Their contribution to rainfall and associated trends was analysed using two combined satellite-rain-gauge precipitation products (PERSIANN and IMERG) and daily rain-gauge data for northern Somalia and Djibouti. Based on case studies and a statistical analysis of rainfall amounts with respect to the distance to the TC center, it was found that rainfall was influenced by TCs over a wide area (up to 750 km from the center), and that heavy rains still occurred one to two days after the TC lifecycle. Despite the rare occurrence of tropical systems (1.5 per year, whatever the category, with a third making landfall), they strongly contribute (30-50%) to mean annual rainfall over the northwestern Arabian Sea, Gulf of Aden and their respective coastlines. On a seasonal basis, this contribution is even higher (40-60 %) in southern Arabia and the adjacent oceanic areas, for both cyclonic seasons (May-June and September-December). High values were also found at the Gulf of Aden stations in Somalia in SOND. Over inland northern Somalia, contributions are lower in MJ

(generally <5%) and SOND (5 to 20%, increasing eastwards). In a belt running northeastward from the Gulf of Aden, a large proportion (30-70%) of heavy rain days (>40 mm) are associated with TCs. In northern Somalia, many 24-hr maximum rainfall amounts are TC-related.

From 1990 to 2020, the number of tropical systems showed a marked increase in the region, hence their enhanced contribution to rainfall totals. Part of the overall upward rainfall trend over the northwestern Arabian Sea, is actually the outcome of increasing cyclonic activity. Though over the Gulf of Aden and neighbouring regions of the Horn of Africa (northern Somalia, Djibouti), TCs are very infrequent, the trend in TC-related rainfall shows a consistent and significant increase, highlighted by the contrast between the subperiods 1990-2007 and 2008-2020. Both cyclonic seasons are involved in this increase. The increase in TC frequency is related to a SST increase in the eastern and southern Arabian Sea, a decrease in vertical wind shear, and a strong increase in tropospheric moisture content.

Some caution should be exerted on the interpretation of these trends, which may not necessarily reflect the effect of anthropogenic climate change. Murakami et al (2013) noted that, under increased greenhouse gases scenarios, a future westward shift of the mean locations of tropical storms is projected over the North Indian Ocean during the post-monsoon season (matching the recent increase in TC days in the WAS). Murakami et al. (2017) found that anthropogenic forcing has likely increased the probability of post-monsoon severe cyclonic storms over the Arabian Sea. Wang et al. (2023) likewise found a potentially dominant role of anthropogenic forcing on coastal TC frequency changes in many basins of the world, including the western coast of the Arabian Sea, but for the latter region their simulations failed to specifically attribute these changes to the effect of aerosol or greenhouse gases. Additionally, the low number of TCs in the early part of the period should also be considered in a broader context, since Rajeevan et al. (2013) showed a decrease in the frequency of intense TCs in the Arabian Sea from the period 1955-1973 to 1974–1992, suggesting large decadal-scale variability in the basin. Evan and Camargo (2011) questioned spurious increases in Arabian Sea TC intensity , which could explain part of the rise in cyclonic storm days they noted between 1979-1991 and 1992-2008 over the Arabian Sea as a whole. Duplicating this study for future periods is now needed, although this discussion highlights that internal climate variability cannot be neglected to obtain robust projections of TC activity, and their impacts on rainfall. Large ensembles from the CMIP6 (Eyring et al. 2016) or MENA-CORDEX (Bucchignani et al. 2015) modelling exercises could be used for that purpose.

Acknowledgements

The authors thank the National Meteorological Agency (ANM) of Djibouti for the provision of daily rainfall data for the Republic of Djibouti and SWALIM for northern Somalia. SWALIM is a project

managed by FAO with funding from The European Union, The Swiss Agency for Development and Cooperation, The Italian Cooperation, DFID, USAID and the Government of France. Calculations were performed using HPC resources from DNUM CCUB (Centre de Calcul de l'Université de Bourgogne).

References

Abdalla, O., & Al-Abri, R. B. Y. (2011). Groundwater recharge in arid areas induced by tropical cyclones: lessons learned from Gonu 2007 in Sultanate of Oman. *Environmental Earth Sciences*, *63*, 229-239.

Akhila, R.S., Kuttippurath, J., Rahul, R. *et al.* (2022). Genesis and simultaneous occurrences of the super cyclone Kyarr and extremely severe cyclone Maha in the Arabian Sea in October 2019. *Nat Hazards 113*, 1133–1150. https://doi.org/10.1007/s11069-022-05340-9

Al-Manji, S., Mitchell, G., and Al Ruheili, A. (2021). Arabian Sea Tropical Cyclones: A Spatio-Temporal Analysis in Support of Natural Hazard Risk Appraisal in Oman. in R.S. Meena (ed.) : Agrometeorology. IntechOpen. doi:10.5772/intechopen.96961.

Ashouri, H., Hsu, K. L., Sorooshian, S., Braithwaite, D. K., Knapp, K. R., Cecil, L. D., ... & Prat, O. P. (2015). PERSIANN-CDR: Daily precipitation climate data record from multisatellite observations for hydrological and climate studies. *Bulletin of the American Meteorological Society, 96(1)*, 69-83.

Baburaj, P.P., Abhilash, S., Mohankumar, K., Sahai, A.K. (2020). On the epochal variability in the frequency of cyclones during the pre-onset and onset phases of the monsoon over the North Indian Ocean. *Advances in Atmospheric Sciences, 37,* 634-651.

Bell, S.S., Chand, S.S., Tory, K.J., Ye, H. and Turville, C. (2020) North Indian Ocean tropical cyclone activity in CMIP5 experiments: future projections using a model-independent detection and tracking scheme. *International Journal of Climatology, 40(15),* 6492–6505. https://doi.org/10.1002/joc.6594.

Breña-Naranjo, J.A., Pedroso-Acuña, A., Pozos-Estrada, O., Jiménez-López, S.A., López-López, M.R. (2015). The contribution of tropical cyclones to rainfall in Mexico. *Physics and Chemistry of the Earth*, Parts A/B/C, 83-84, 111-122.

Bucchignani, E., Mercogliano, P., Rianna, G., Panitz, H.J. (2015). Analysis of ERA-Interim-driven COSMO-CLM simulations over Middle East – North Africa domain at different spatial resolutions – *International Journal Of Climatology* DOI: 10.1002/joc.4559

691 Chazée, L. (2017). *Patrimoine socio-économique et naturel de la région du Cap Gardafui*.
692 L'Harmattan, Paris, 330 p.

693 Cherel, J. P., Omar Ali, B., Nour Ayeh, M., & Vinet, F. (2020). Activités cycloniques et nouveaux
694 risques dans le golfe d'Aden. Exemple des impacts socio-économiques du cyclone Sagar sur Djibouti
695 en mai 2018. *EchoGéo*, 51. https://doi.org/10.4000/echogeo.18859

696 Deo, A.A., Ganer, D.W. & Nair, G. (2011). Tropical cyclone activity in global warming scenario. *Nat*
697 *Hazards 59*,771–786.

698 Deshpande, M., Singh, V. K., Ganadhi, M. K., Roxy, M. K., Emmanuel, R., & Kumar, U. (2021). Changing
699 status of tropical cyclones over the north Indian Ocean. *Climate Dynamics*, *57*, 3545-3567.

700 Englehart, P. J., & Douglas, A. V. (2001). The role of eastern North Pacific tropical storms in the
701 rainfall climatology of western Mexico. *International Journal of Climatology, 21(11)*, 1357-1370.

702 Evan, A. T., & Camargo, S.J. (2011). A Climatology of Arabian Sea Cyclonic Storms. *J. Climate, 24,* 140–
703 158.

704 Evan, A. T., Kossin, J. P., Chung, C. E. & Ramanathan, V. (2021). Arabian Sea tropical cyclones
705 intensified by emissions of black carbon and other aerosols. *Nature 479,* 94–97.

706 Eyring, V., Bony, S., Meehl, G. A., Senior, C. A., Stevens, B., Stouffer, R. J., and Taylor, K. E. (2016).
707 Overview of the Coupled Model Intercomparison Project Phase 6 (CMIP6) experimental design and
708 organization. *Geosci. Model Dev., 9,* 1937–1958, https://doi.org/10.5194/gmd-9-1937-2016.

709 Finney, D. L., Marsham, J. H., Walker, D. P., Birch, C. E., Woodhams, B. J., Jackson, L. S., & Hardy, S.
710 (2020). The effect of westerlies on East African rainfall and the associated role of tropical cyclones
711 and the Madden–Julian Oscillation. *Quarterly Journal of the Royal Meteorological Society, 146(727)*,
712 647-664.

713 Fors, J.R. (1977). *Tropical cyclone Kathleen*. NOAA Technical Memorandum NWS WR-114, 29 p.

714 Gaona, M. F. R., Villarini, G., Zhang, W., & Vecchi, G. A. (2018). The added value of IMERG in
715 characterizing rainfall in tropical cyclones. *Atmospheric Research, 209*, 95-102.

716 Gray, W. M. (1968). Global view of the origin of tropical disturbances and storms. *Mon. Wea. Rev.,*
717 *96*, 669–700.

718 Hari, V., Pathak, A., & Koppa, A. (2021). Dual response of Arabian Sea cyclones and strength of Indian
719 monsoon to Southern Atlantic Ocean. *Climate Dynamics, 56,* 2149-2161.

720 Hoarau, K., Bernard, J., & Chalonge, L. (2012). Intense tropical cyclone activities in the northern
721 Indian Ocean. *International journal of climatology*, *32(13)*, 1935-1945.

722 Huffman, G. J., Bolvin, D. T., Nelkin, E. J., & Tan, J. (2015). Integrated Multi-satellitE Retrievals for
723 GPM (IMERG) technical documentation. *Nasa/Gsfc Code, 612(47*), 2019.

724 IFRC (2013). International Federation of Red Cross and Red Crescent Disaster Relief Emergency Fund :
725 Somalia Tropical Cyclone. https://reliefweb.int/report/somalia/somalia-tropical-cyclone-dref-
726 operation-n-mdrso002-update-no-1 Accessed 25 September 2023.

727 Jiang, H., & Zipser, E. J. (2010). Contribution of tropical cyclones to the global precipitation from eight
728 seasons of TRMM data: Regional, seasonal, and interannual variations. *Journal of climate, 23(6),*
729 1526-1543.

730 Kabir, R., Ritchie, E.A., Stark, C. (2022). Tropical Cyclone Exposure in the North Indian Ocean.
731 *Atmosphere*, *13*, 1421. https://doi.org/10.3390/atmos13091421

732 Kebacho, L. L. (2022). The role of tropical cyclones Idai and Kenneth in modulating rainfall
733 performance of 2019 long rains over East Africa. *Pure and Applied Geophysics, 179(4)*, 1387-1401.

734 Khouakhi, A., Villarini, G., Vecchi, G.A. (2017). Contribution of Tropical Cyclones to Rainfall at the
735 Global Scale. *J. Climate*, *30*, 359–372.

736 Knapp, K. R., Kruk, M. C. , Levinson, D. H. , Diamond, H. J., and Neumann, C. J. (2010). The
737 International Best Track Archive for Climate Stewardship (IBTrACS): Unifying tropical cyclone best
738 track data. *Bulletin of the American Meteorological Society, 91*, 363-376.
739 doi:10.1175/2009BAMS2755.1

740 Knapp, K. R., Diamond, H. J., Kossin, J. P. , Kruk, M. C., Schreck, C. J. (2018). *International Best Track*
741 *Archive for Climate Stewardship (IBTrACS) Project, Version 4*. NOAA National Centers for
742 Environmental Information. doi:10.25921/82ty-9e16 [accessed 23 February 2024].

743 Knutson, T.R., Sirutis, J.J., Zhao, M., Tuleya, R.E., Bender, M., Vecchi, G.A., Villarini, G. and Chavas, D.
744 (2015). Global projections of intense tropical cyclone activity for the late twenty-first century from
745 dynamical downscaling of CMIP5/RCP4.5 scenarios. *Journal of Climate, 28(18)*, 7203–7224.
746 https://doi.org/10. 1175/JCLI-D-15-0129.1.

747 Kpanou, M., Laux, P., Brou, T., Vissin, E., Camberlin, P., & Roucou, P. (2021). Spatial patterns and
748 trends of extreme rainfall over the southern coastal belt of West Africa. *Theoretical and Applied*
749 *Climatology*, *143*, 473-487.

Lavender, S.L., McBride, J.L. (2021). Global climatology of rainfall rates and lifetime accumulated rainfall in tropical cyclones: Influence of cyclone basin, cyclone intensity and cyclone size. *Int J Climatol. 41 (Suppl. 1)*: E1217–E1235.

Lvončík, S., Vahalík, P., Bongers, F. et al. (2020). Development of a population of Boswellia elongata Balf. F. in Homhil nature sanctuary, Socotra island (Yemen). *Rend. Fis. Acc. Lincei 31,* 747–759. https://doi.org/10.1007/s12210-020-00936-4

Murakami, H., Sugi, M. and Kitoh, A. (2013). Future changes in tropical cyclone activity in the north Indian Ocean projected by high-resolution MRI-AGCMs. *Climate Dynamics, 40(7–8),* 1949–1968. https://doi.org/10.1007/s00382-012-1407-z.

Murakami, H., Vecchi, G. A., and Underwood, S. (2017). Increasing frequency of extremely severe cyclonic storms over the Arabian Sea. *Nature Climate Change*, *7[12]*, 885–889.

Neumann, C.J. (2017). A Global Tropical Cyclone Climatology. In WMO *Global Guide to Tropical Cyclone Forecasting*, 28-62. https://cyclone.wmo.int/pdf/Global-Guide-to-Tropical-Cyclone-Forecasting.pdf

Ng, B., Walsh, K., Lavender, S. (2014). The contribution of tropical cyclones to rainfall in northwest Australia. *International Journal of Climatology, 35 (10),* 2689-2697. https://doi.org/10.1002/joc.4148

OCHA Somalia (2020). *Somalia, Tropical Cyclone Gati Update #2. ReliefWeb. UN Office for the Coordination of Humanitarian Affairs. 24 November 2020*. https://reliefweb.int/report/somalia/ocha-somalia-tropical-cyclone-gati-update-2-24-november-2020 Accessed 5 December 2023

Owuor, A., & David McRae, H. (2022). The Control of the Desert Locusts (Schistocerca gregaria) in Somalia during the Upsurge Between 2019 and 2021. *Outlooks on Pest Management, 33(6),* 221-226.

Pedgley, D. E. (1969). Cyclones along the Arabian coast. *Weather, 24(11)*, 456-470.

Pillay, M. T., & Fitchett, J. M. (2021). On the conditions of formation of Southern Hemisphere tropical cyclones. *Weather and Climate Extremes, 34*, 100376.

Prat, O. P., & Nelson, B. R. (2013). Mapping the world's tropical cyclone rainfall contribution over land using the TRMM Multi-satellite Precipitation Analysis. *Water Resources Research, 49(11),* 7236-7254.

Priya, P., Pattnaik, S. & Trivedi, D. (2022). Characteristics of the tropical cyclones over the North Indian Ocean Basins from the long-term datasets. *Meteorol Atmos Phys 134*, 65. https://doi.org/10.1007/s00703-022-00904-7

Rajeevan, M., Srinivasan, J., Niranjan Kumar, K., Gnanaseelan, C., & Ali, M. M. (2013). On the epochal variation of intensity of tropical cyclones in the Arabian Sea. *Atmospheric Science Letters, 14(4),* 249-255.

Ramsay, H. (2017). The Global Climatology of Tropical Cyclones. *Oxford Research Encyclopedia of Natural Hazard Science.* Retrieved 31 Aug. 2023, from https://oxfordre.com/naturalhazardscience/view/10.1093/acrefore/9780199389407.001.0001/acrefore-9780199389407-e-79.

Résumé Mensuel du Temps (1972). *Résumé mensuel du temps en Territoire Français des Afars et des Issas*, Service de la Météorologie, Djibouti, Octobre 1972, 14 p.

Ray-Choudhuri, S., Subramanyan, Y. H., & Chellappa, R. (1959). A climatological study of storms and depressions in the Arabian Sea. *Mausam, 10(3)*, 283-290.

Roy Chowdhury, R., Prasanna Kumar, S., Narvekar, J., & Chakraborty, A. (2020). Back-to-back occurrence of tropical cyclones in the Arabian sea during October–November 2015: causes and responses. *Journal of Geophysical Research: Oceans, 125(6),* e2019JC015836.

Salih, A. A., Baraibar, M., Mwangi, K. K., & Artan, G. (2020). Climate change and locust outbreak in East Africa. *Nature Climate Change, 10(7)*, 584-585.

Sattar, A. M., & Cheung, K. K. (2019). Comparison between the active tropical cyclone seasons over the Arabian Sea and Bay of Bengal. *International Journal of Climatology, 39(14),* 5486-5502.

Schreck, C.J., Knapp, K.R., Kossin, J.P. (2014). The impact of best track discrepancies on Global Tropical Cyclone climatologies using IBTrACS. *Monthly Weather Review, 142*, 3881-3899.

Shanko, D., & Camberlin, P. (1998). The effects of the Southwest Indian Ocean tropical cyclones on Ethiopian drought. *International Journal of Climatology*, *18(12),* 1373-1388.

Singh, K., Panda, J. & Mohapatra, M. (2020). Robustness of best track data and associated cyclone activity over the North Indian Ocean region during and prior to satellite era. *J Earth Syst Sci 129*, 84. https://doi.org/10.1007/s12040-020-1344-x

Singh, V. K., & Roxy, M. K. (2022). A review of ocean-atmosphere interactions during tropical cyclones in the north Indian Ocean. *Earth-Science Reviews, 226*, 103967.

Tiwari, G., Kumar, P., Javed, A., Mishra, A. K., & Routray, A. (2022). Assessing tropical cyclones characteristics over the Arabian Sea and Bay of Bengal in the recent decades. *Meteorology and Atmospheric Physics*, *134(3)*, 44.

Wahiduzzaman, M., Cheung, K., Luo, J. J., Bhaskaran, P. K., Tang, S., & Yuan, C. (2022). Impact assessment of Indian Ocean Dipole on the North Indian Ocean tropical cyclone prediction using a Statistical model. *Climate Dynamic*s, *58*, 1275–1292. https://doi.org/10.1007/s00382-021-05960-0

Wang, B., Xu, S. & Wu, L. (2012). Intensified Arabian Sea tropical storms. *Nature 489*, E1–E2 https://doi.org/10.1038/nature11470.

Wang, S., Murakami, H. & Cooke, W.F. (2023). Anthropogenic forcing changes coastal tropical cyclone frequency. *npj Clim Atmos Sci 6*, 187. https://doi.org/10.1038/s41612-023-00516-x

Yuan, J., Cao, J. (2013). North Indian Ocean tropical cyclone activities influenced by the Indian Ocean Dipole mode. *Sci. China Earth Sci. 56*, 855–865. https://doi.org/10.1007/s11430-012-4559-0